공학석사 학위논문

Nonlinear Model Predictive Control for Gas Antisolvent Recrystallization Process

기체 역용매 재결정화 공정의 비선형 모델예측제어

2013년 2월

서울대학교 대학원
화학생물공학부
이 신 제

Nonlinear Model Predictive Control for Gas Antisolvent Recrystallization Process

지도교수 이 종 민

이 논문을 공학석사 학위논문으로 제출함

2012년 12월

서울대학교 대학원

화학생물공학부

이 신 제

이 신 제의 석사 학위논문을 인준함

2012년 12월

위 원 장 _____ (인)

부위원장 _____ (인)

위 원 _____ (인)

Abstract

Nonlinear Model Predictive Control for Gas Antisolvent Recrystallization Process

Shin Je Lee
School of Chemical and Biological Engineering
The Graduate School
Seoul National University

Crystallization techniques have been played an important role for several decades in producing various chemical products such as polymers, dyes, pharmaceuticals, and explosives. It is also essentially used in separation and purification stages of petrochemical and fine-chemical industries. Conventional crystallization processes, however, have practical problems in that toxic waste solvent streams are inevitably produced in the process and some substances are contaminated with the solvent, deteriorating the purity. In this reason, novel crystallization processes using supercritical fluids have recently attracted much attention. They are environmentally acceptable due to the use of benign solution such as CO_2, applicable to various solutes, and operated at mild conditions, 25°C and 5-100 bar. These include rapid expansion of supercritical solution (RESS), gas antisolvent (GAS) process, and particles from gas-saturated solutions (PGSS).

It is well known that GAS crystallization process attains a very rapid, essentially uniform and very high supersaturation upon reduction of the solid solubility in its solution with dissolution of antisolvent CO_2. This owes to the two way mass transfer of CO_2 and solvent, for dissolution of CO_2 and evaporation of solvent, respectively. This facilitates uniform nucleation and almost instantaneous crystallization, which make the antisolvent crystallization a unique process resulting in the formation of ultra-fine particles with a narrow particle size distribution and controlled morphology.

In this work, a dynamic model for GAS process is presented and control approach to obtain a desired particle size distribution (PSD) is proposed. At first, a mathematical model from a population balance model (PBM) is developed to describe PSD of GAS process. The developed GAS model consists of a partial differential equation (PDE), a set of ordinary differential equations (ODE), and algebraic equations associated with it. Thus, it requires a numerical discretization method to solve the PDE. A high resolution (HR) scheme is presented since it is rather simple to implement and more accurate than other discretization methods. Simulation results show the effect of CO_2 addition rate on the final particle size distribution in the process.

Control issues in GAS processes are quite challenging since the system is highly nonlinear and includes complex crystallization kinetics, nucleation and growth. Researchers have investigated the control of liquid antisolvent crystallization process to find optimal input profile, but the control for gas antisolvnet process has not been much tried yet. It is generally more difficult to control GAS process than liquid antisolvent process since the liquid-vapor

phase equilibrium should be considered in the system model. A nonlinear model predictive control (MPC) strategy is proposed to control the particle size distribution of GAS process. Linear MPC, successive linearized MPC are applied to the system and the control results are compared.

Keywords: Gas antisolvent recrystallization, Population balance model, High resolution method, Model predictive control

Student Number: 2011-21062

Contents

List of Figures

List of Tables

Chapter 1

Introduction

Crystallization is a formation process of a solid state of matter in which the molecules are arranged in a regular pattern. Solid crystals generally precipitate from a solution, melt or gas. Crystallization is also a process of chemical solid–liquid separation, in which mass transfer of a solute from the liquid phase to a pure crystalline phase occurs. This technique has been at some stage in nearly all process industries for decades as a method of production, purification, and recovery of solid materials. In recent years, a number of new applications also rely on crystallization processes such as the production of nano and amorphous materials. Crystallization have experienced major advances in the past years and well establised in both academic and industrial areas.

1.1 Crystallization process in industry

Crystallization plays a huge role in producing various chemical products such as polymers, dyes, pharmaceuticals, and explosives. It is also widely used to separate and purify chemical species in the petrochemical and fine-chemical industries. DuPont, one of the world's largest chemical companies,

estimated in 1988 [1] that approximately 70% of its products pass through crystallization or precipitation stage. Crystallization process is a particularly consequential for the pharmaceutical industry since most pharmaceuticals are produced in a solid form. Crystallization is also used to identify structure for use in drug design, to isolate chemical species from mixtures of reaction products, and to achieve consistent and controlled drug delivery. In the semiconductor industry, crystallization thechnique is used to grow long, cylindrical, single crystals of silicon with a mass of several hundred kilograms. These gigantic crystals, called boules, are sliced into thin wafers upon which integrated circuits are etched. In the food industry, crystallization is often used to give products the right texture, flavor, and shelf life when producing frozen dried foods, butter, salt, and cheese [2].

These industrial examples highlight the importance of manufacturing solids having desirable and consistent properties. Therefore, achieving good control performance over crystallization processes is one of the significant issues in this area.

1.2 Crystallization mechanism

The basic principle of crystallization process is examined in this section by inspecting the method of solution crystallization. The physical system of solution crystallization consists of one or more solutes dissolved in a solvent. The system can be undersaturated, saturated, or supersaturated with respect to species i, depending on whether the solute concentration c_i is less than, equal to, or greater than the saturation concentration c_i^*. Crystallization

occurs only if the system is at the supersaturation state, where the solute concentration exceeds the saturation concentration as shown in Fig. 1. The supersaturation level is commonly expressed as either

$$\sigma = \frac{c_i - c_i^*}{c_i^*}, \tag{1.1}$$

$$S = \frac{c_i}{c_i^*}, \tag{1.2}$$

$$\text{or,} \quad \Delta c = c_i - c_i^* \tag{1.3}$$

where σ, S, and Δc indicate supersaturations.

The supersaturation level can be increased by lowering the saturation concentration from cooling or by increasing the solute concentration from evaporation of the solvent. Crystallization moves a supersaturated solution toward equilibrium by transferring solute molecules from the liquid phase to the solid phase. This process is initiated by nucleation, which is the birth or initial formation of a crystal. Nucleation occurs, however, only if the necessary activation energy is supplied. A supersaturated solution in which the activation energy is too high for nucleation to occur is called metastable. As the supersaturation level increases, the activation energy decreases. Thus spontaneous nucleation, also called primary nucleation, occurs only at sufficiently high levels of supersaturation, and the solute concentration at which this nucleation occurs is called the metastable limit (C).

Since primary nucleation is difficult to control reliably, primary nucleation is often avoided by injecting crystal seeds into the supersaturated solution. Crystal nuclei and seeds provide a surface for crystal growth to

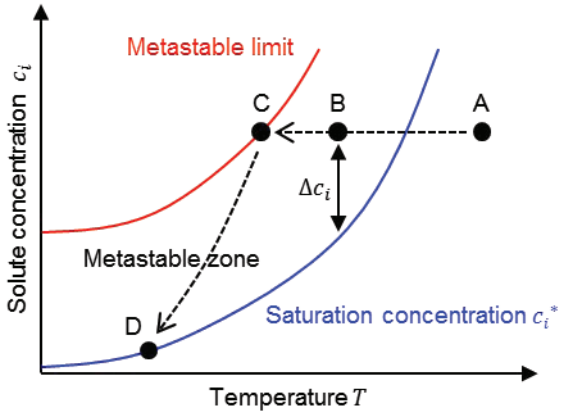

Figure 1: Crystallization mechanism

occur. Crystal growth involves solute molecules attaching themselves to the surfaces of the crystal according to the crystalline structure.

Crystals suspended in a well-mixed solution can collide with each other or with the crystallizer internals, causing crystal attrition and breakage, which results in additional nuclei. Nucleation of this type is called secondary nucleation.

The rates at which crystal nucleation and growth occur are functions of the supersaturation level. The goal of crystallization control is to balance the nucleation and growth rates to achieve the desired crystal size objective which is often uniformly sized crystals. Well-controlled crystallization processes operate in the metastable zone, between the saturation concentration and the metastable limit, to promote crystal growth while minimizing undesirable primary nucleation [2].

1.3 Crystallization techniques using supercritical fluids

Conventional crystallization processes have been well established in a variety of industries as mentioned in the previous section, however, there are several practical problems associated with the processes. Some substances are contaminated with solvent in recrystallization processes, and waste solvent streams are inevitably produced in most processes, and the worst problem is that the waste organic streams are toxic to the environment. Applying supercritical fluids can overcome the drawbacks of conventional processes. The crystallization processes using supercritical fluids have been intensively studied. The unique thermodynamic and fluid dynamic properties of supercritical fluids makes the system easy to tune and able to operate under mild and inert conditions. The concepts and characteristics of these applications for particle formation are reviewed and organized in [3] and [4].

1.3.1 Rapid expansion of supercritical solutions (RESS)

In rapid expansion of supercritical solutions (RESS), a solute is dissolved in supercritical fluids and the solution is rapidly expanded to lower pressure level which causes the solute to precipitate. This concept has been demonstrated for a wide variety of materials including polymers, dyes, and pharmaceuticals. A schematic representation of RESS is shown in Fig. 2 and the process flow in detail is illustrated below.

At first, the pure carbon dioxide is pumped to the desired pressure and preheated to extraction temperature through a heat exchanger to convert the

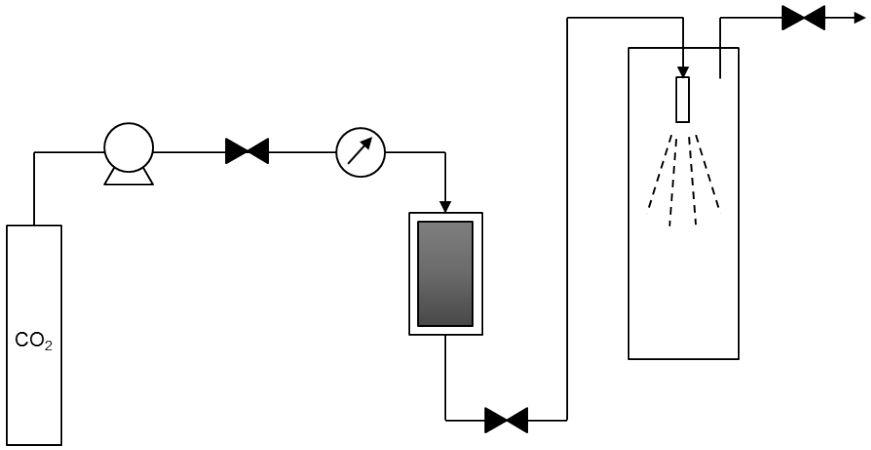

Figure 2: Schematic representation of RESS

normal CO_2 into the supercritical fluid. The supercritical fluid then dissolves the target solute at high pressure in an autoclave. In the precipitation unit, the supercritical solution is expanded through a nozzle that must be reheated to avoid plugging by solute precipitation.

One key parameter of RESS is the nozzle geometry, of which two types are used, a capillary of 100 μm and laser drilled nozzles of 20-60 μm diameter. Other important parameters of this process include temperature, pressure drop, dimensions of the micronization vessel [5], [6], [7], [8], [9].

RESS has several advantages; very fine particles of some nanometers can be produced with solvent-free, and it is simple and relatively easy to implement at small scale when a single nozzle is used. However, extension to a production size requires either a multi-nozzle system or use of a porous sintered disk through which pulverization occurs. Controlling particle size distribution is not easy in both cases and the additional equipment complicates the particle collection. But the most important limitation of RESS

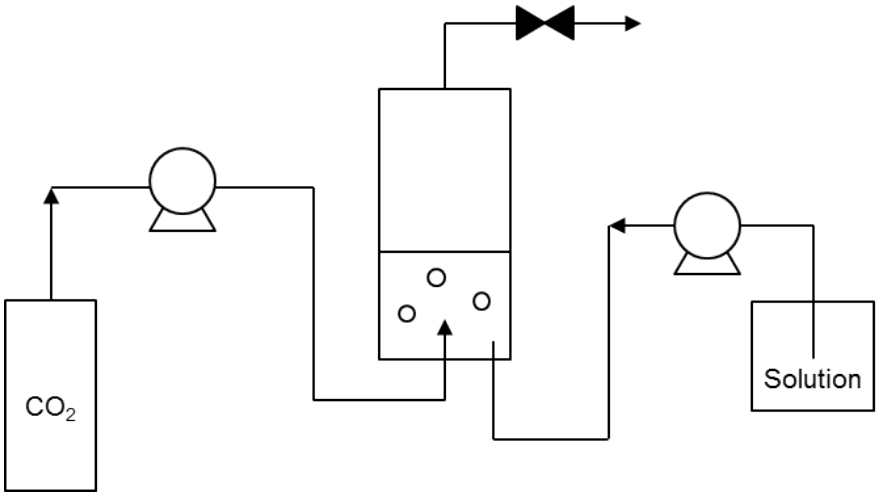

Figure 3: Schematic representation of GAS process

process lies in that most attractive compounds are not soluble enough into the supercritical fluid to leak to profitable processes. A co-solvent may be used to improve this solubility, but it also requires another separation device to harvest crystals from it. In recent years, the research to find the appropriate supercritical solvent able to dissolve the solute has actively carried out.

1.3.2 Gas antisolvent process (GAS)

The application of supercritical fluids as antisolvents can be an alternative for producing solids that are insoluble in supercritical fluids. In gas antisolvent recrystallization process, the antisolvent lowers the solvent strength and precipitates the solute dissolved initially in a liquid solvent. The conceptual equipment is presented in Fig. 3 and the particle formation procedure in GAS process is illustrated in Fig. 4.

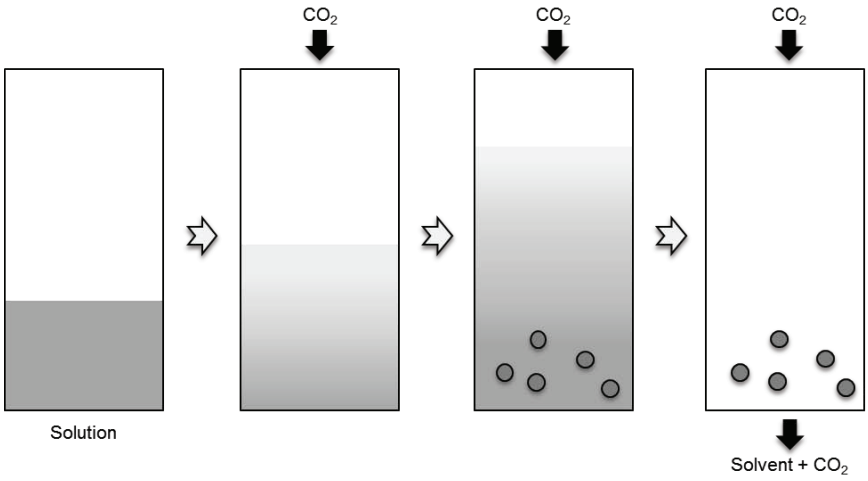

Figure 4: Particle formation steps of GAS process

In this method, a solution dissolved with the solute is initially loaded in a precipitator. CO_2 is pumped up to high pressure over its critical point and injected into the vessel from the bottom to achieve a better mixing of the solvent and antisolvent. Then, the solution is expanded and has a lower solvent strength than the pure one. Thus, the expanded solution becomes supersaturated and particles are crystallized. After a holding time, the solution is drained under isobaric conditions to wash and collect particels.

It is demonstrated that the antisolvent addition rate may be programmed to control particle size, size distribution and morphology by Gallagher [10]. Temperature and initial solution concentration have also an effect on the final crystal quality, however, the antisolvent addition rate is found to have the strongest impact on the final product [11].

Very small particles can be obtained using GAS process and the particle sizes are easily controlled in this method. Above all, it is applicable for

almost any kind of compounds unlike RESS. Antisolvent processes have potential especially for drug delivery systems. Nevertheless, scale-up is not well known and presently foreseen only for high-value specialty materials such as pharmaceuticals, cosmetics, and superconductors with a small amount of production. Particle separation from residual organic solvent is also a shortcoming in this technique. Even separation of antisolvent and solvent may be required in an industrial application [3], [4].

1.3.3 Particles from gas-saturated solutions (PGSS)

One goal of RESS and GAS process is to obtain very small particles with size of micron. Although their scale-up strategies are not yet very well known, they have possibilities for producing relatively small amounts of high value-added products. On the other hand, particles from gas-saturated solutions (PGSS) process can be applied for large scale production even if the obtained particles are not of submicron size. The process already runs in plants with a capacity of several hundred kilograms per hour [4].

As the solubilities of compressed gases in liquids and solids like polymers are usually high, and much higher than the solubilities of such liquids and solids in the compressed gas phase, the process consists in solubilizing supercritical carbon dioxide in melted or liquid-suspended substances, leading to a so-called gas-saturated solution that is further expanded through a nozzle with formation of solid particles, or droplets as shown in Fig. 5. Typically, this process allows to form particles from a great variety of substances that need not to be soluble in supercritical carbon dioxide [12], [13], [14]. This process can also be used with suspensions of active solutes in a

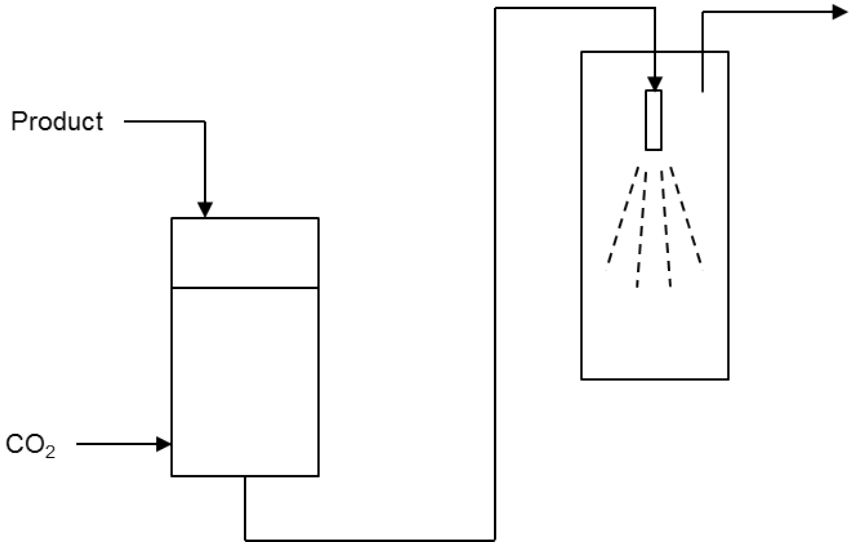

Figure 5: Schematic representation of PGSS

polymer or other carrier substance leading to composite microspheres [3].

Particle formation using the PGSS concept is already widely used at large scale as mentioned earlier. The simplicity of this concept leads to low processing costs, and thus easy industrial applications. The very wide range of products that can be treated also progresses development of PGSS process applications, not only for high-value materials but also for commodities, in spite of limitations related to the difficulty to monitor particle size.

Technological features of RESS, GAS process, and PGSS process are summarized and compared in Table 1 [4].

1.4 Control issues for crystallization process

Advances in crystallization process control have been enabled by progress in in-situ real-time sensor technologies and driven primarily by needs in the

Table 1: Technological features of RESS, GAS, and PGSS processes [4]

	RESS	GAS	PGSS
Establishing gas-containing solution	Discontinuous	Semicontinuous	Continuous
Gas demand	High	Medium	Low
Pressure	High	Low to medium	Low to medium
Solvent	None	Yes	None
Volume of pressurezed equipment	Large	Medium to large	Small
Separation gas/solid	Difficult	Easy	Easy
Separation gas/solvent	Not required	Difficult	Not required

pharmaceutical industry for improved and more consistent quality of drug crystals [15]. These advances include the accurate measurement of solution concentrations and crystal characteristics as well as the first-principles modeling and robust model-based feedback control of crystal size and distribution. The model-based optimal control formulations applied for decades to continuous crystallization have limitations in terms of optimization objectives and constraints, optimization variables, and methods of dealing with uncertainties. Reseaches have been progressed to remove these limitations and to consider new crystal product quality characteristics and optimization variables. Fig. 6 shows the generic formulation of the model-based crystallization control approach as an optimization problem that indicates the typical optimization objectives, optimizaiton variables, and constraints.

The optimization is subject to model equations and various constraints owing to equipment limitations (e.g., maximum and minimum temperature values, maximum and minimum cooling rates, maximum volume, limits on antisolvent addition rate), productivity requirements (to ensure a desired yield at the end of the batch), and quality specifications [16], [17], [18].Usually the optimization objectives such as the number-average crys-

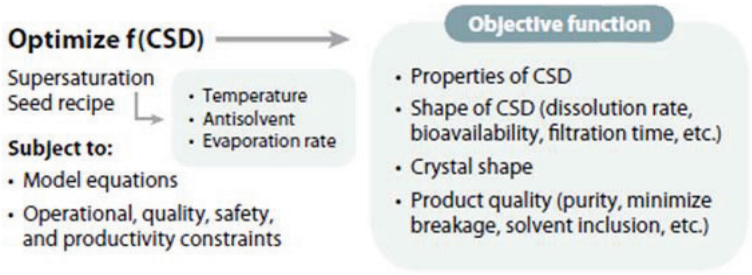

Figure 6: Optimization problem formulation of the model-based crystallization control

tal size, coefficient of variation, nucleated-to-seed-mass ratio, and weight-mean size can be computed efficiently using the method of moments, but the optimal operating conditions and their robustness may depend strongly on the objective [19], [20], [21]. A major advance in the application of model-based control approaches is the development of comprehensive uncertainty analysis and robust optimization formulations that are able to account for the effects of realistic uncertainties and disturbances on optimal operating policies [15].

Improvement of robust performance can be achieved by repeating the optimization on-line on the basis of real-time measurements and state estimation, which is known as model predictive control [22], [23].

In this work, we propose model predictive control approaches to control the particle size distribution of GAS process. Controlling the PSD of GAS process can be challenging because the system shows highly nonlinear behavior and includes complex liquid-vapor phase equilibrium. Successive liniearized MPC is applied to the process to handle the nonlinear character-

istics.

1.5 Outline of the thesis

The thesis includes the followings. In Chapter 2, the experimental part of GAS process is provided, describing the target material, equipments, and the experimental results. The effect of CO_2 addition rate on PSD is mainly investigated.

Modeling procecure and simulation are given in Chapter 3. A mathematical model from a population balance model (PBM) is developed to describe particle size distribution of GAS process. The developed GAS model consists of a partial differential equation, a set of ordinary differential equations, and algebraic equations associated with it. Thus, it requires a numerical discretization method to solve the PDE. A high resolution (HR) scheme is used because it is rather simple to implement and more accurate than other discretization methods. Simulation results are also represented in this chapter and the effect of CO_2 addition rate on the PSD of this system is examined.

In Chapter 4, A nonlinear model predictive control (MPC) strategy is presented to obtain the desired particle size distribution of GAS process. Linear MPC and successive linearized MPC are applied to the system and the control results are also compared.

Concluding remarks are presented in Chapter 5, summarizing the main results of the thesis.

Chapter 2

Experiment

In the case of explosives, product quality including properties such as performance and insensitivity, can be significantly influenced by particle size and particle morphology [24]. Many attempts have been made to change the endproduct properties such as crystal phase, particle size, particle size distribution, and morphology to enhace the performance and insensitivity. In general, grinding and crystallization from solution are largely used as crystallization processes for explosives in industry. However, these processes have some limitations; It is not only difficult to control morphology and particle size of explosives, but also dangerous to obtain fine particles because of their vulnerability to heat and impact. Thesedays, using GAS crystallization has attracated interest since it allows the production of nano- or micrometer-sized explosives with controlled morphology, crystal phase, and particle size distribution. HMX (cyclotetramethylenetetranitramine or octahydro-1,3,5,7-tetranitro-1,3,5,7-tetrazocine) is used as a target explosive in the experiment [24], [25].

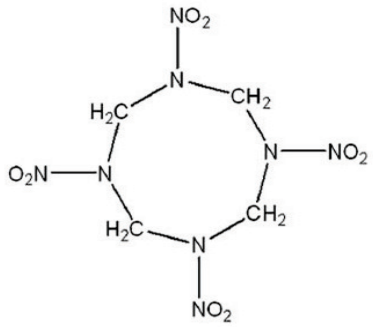

Figure 7: Molecular structure of HMX

2.1 Materials and equipments

Materials

HMX is widely used not only for military purposes but also in industrial applications. It is a white crystalline powder that is practically insoluble in water and highly soluble in organic solvents such as acetone, dimethyl sulfoxide (DMSO), dimethylformamide (DMF), and cyclohexanone. Chemical information and some physical properties of HMX are listed in Table 2. and molecular structure is illustrated in Fig. 7. Fig. 8 shows a SEM image and particle size distribution of raw HMX. It is realized that particle size of raw material is rather large and the PSD is very wide [24], [25].

Table 2: Physical properties of HMX

Property	Value
Molecular formula	$C_4H_8N_8O_8$
Molecular weight	296.2
Crystal density at 20 °C, β-phase	1.96
Melting point (°C)	275
Deflagration point (°C)	287

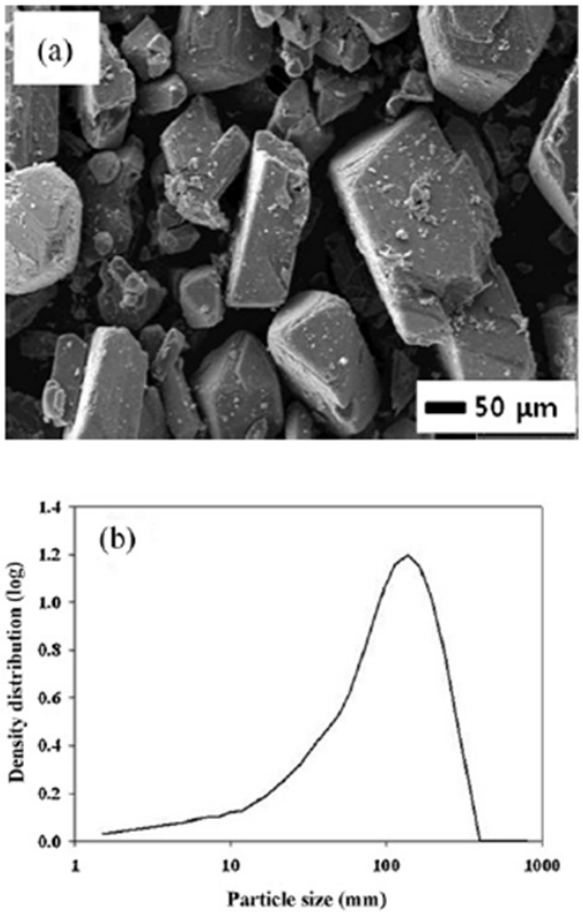

Figure 8: Raw HMX particles; (a) SEM image, (b) Particle size distribution

Equipments

An experimental apparatus for GAS process is represented in Fig. 9. It consisted of a carbon dioxide supply part, solution pump, precipitator, membrane filter, and gas/liquid separator. First, the solution (6) with a constant concentration of the explosive is injected into the precipitator (9) using the solution pump (Mini pump, NSI-33R). After that, CO_2 from the cylinder (1) is sub-cooled by a cooling bath (2) (MC-11, JEIO TECH) and injected into a preheater (4) using the high pressure pump (3) (diagram metering pump). In the preheater, compressed liquid CO_2 is heated to the precipitation temperature and directed to the precipitator. The 150 mL precipitator (9) is made of stainless steel and equipped with two windows, which could withstand high pressure to observe recrystallization activity inside. The temperature of the precipitator is controlled by installing a heat-transfer unit with a water-circulated jacket and the stirrer (8) ($\approx$1000 rpm,) is regulated by a motor controller ensuring well-mixed the solution with CO_2. Two temperature sensors (K-type thermocouple) are placed in the precipitator and the detected temperature is monitored. The pressure of the precipitator is adjusted using a back pressure regulator (5, 12) and measured by a pressure gauge (Max = 500 bar, Millipore). The precipitated explosive particles are collected on a high pressure membrane filter (11) (0.5 μm). The gas/liquid separator (13) was used to collect the organic solvent from the vented CO_2 [26,27]. Particle sizes and their distribution are evaluated by a particle size analyzer (Sympatec model HELOS/BF, Clausthal-Zellerfeld, Germany) that could measure in a size range from 0.1 to 875 μmdepending on the lens (R1, R3, R4, and R5). The powder was placed in the particle size analysis (PSA) system and was allowed to flow into the PSA instrument by the RODOS/M ASPRIOS disperse system [24], [25].

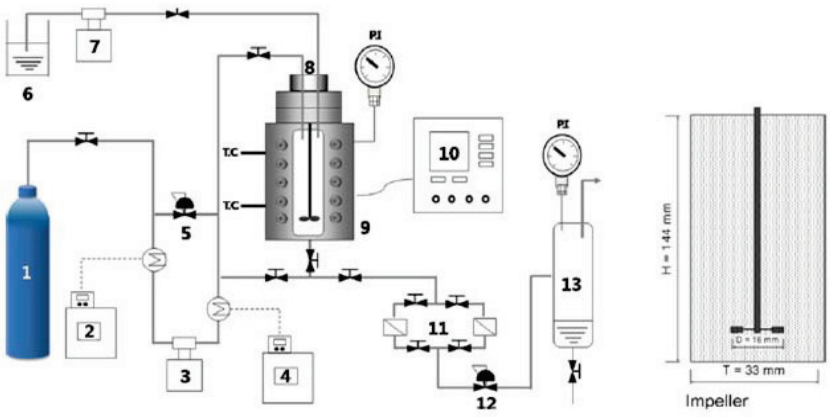

Figure 9: Schematic diagram of experimental apparatus for GAS process

2.2 Experimental results

In this section, experimental results of HMX using GAS crystallization are given. HMX is crystallized by three different solvents, chclohexanone, acetone, and DMF. Then, the effect of temperature on PSD is investgated by operating at 303, 313, and 323K [24], [25].

Fig. 10 shows the particle size distributions of HMX particles obtained from GAS process. The precipitated HMX particles show a variety of particle sizes depending on the organic solvent used. The mean particle sizes of the precipitated HMX particles ranges from 5.3 to 32.1 μm [24], [25].

Volume expansion of liquid solvent is also measured. During injection of CO_2, the volume expansion of solvent is measured by reading the liquid level through the view window. The volume expansion curves for acetone, as shown in Fig. 11, are measured for the determination of pressure-temperature- volume behavior at 303, 313, and 323 K in a vessel of 150 cm^3 equipped with sight glasses. The volume expansion of solvent is strongly affected by temperature. At lower temperature, a higher volume expansion is measured at a given pressure. For example, the volume expansion of ace-

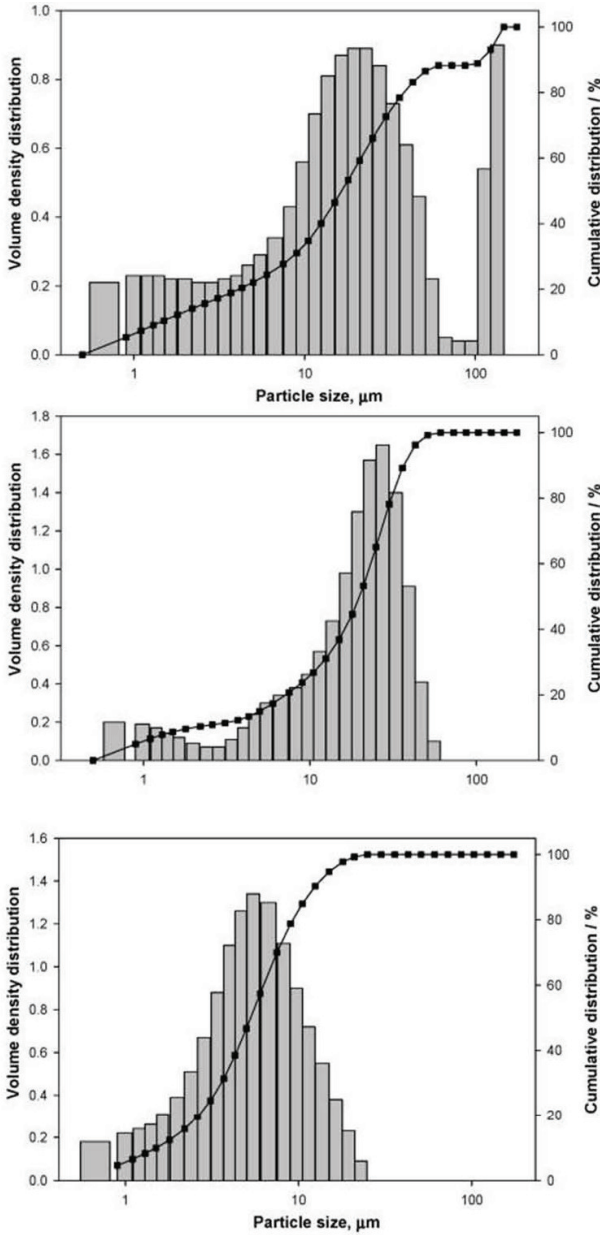

Figure 10: Cumulative size and volume desity distributions of HMX obtained from sholutions (a) cyclohexanone, (b) acetone, and (c) DMF

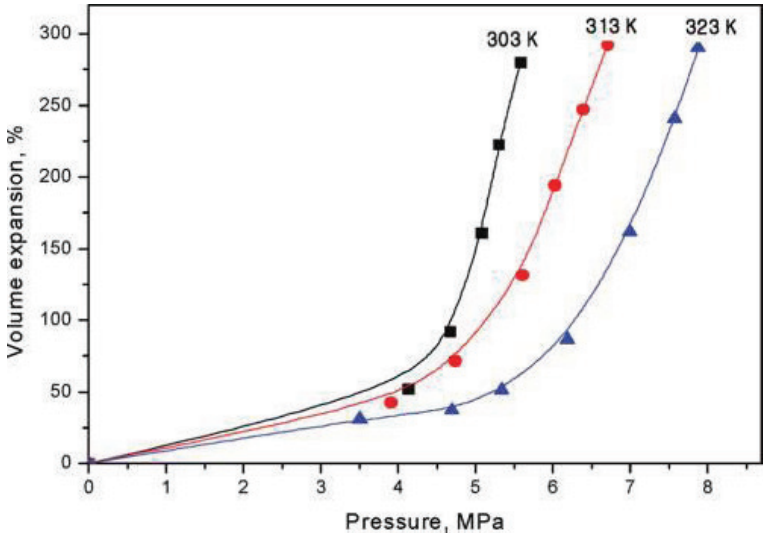

Figure 11: Volume expansion curves of acetone at different temperatuers

tone at 303 K increase to 300% when the pressure is 5.5 MPa. The volume expansion decrease, reaching 48% at 323 K as thetemperature increase [24], [25].

Experiments on the effect of temperature is performed at 303, 313, and 323 K at the CO_2 addition rate of 50 mL^3/min. The resulted SEM images are shown in Fig. 12. The amount of HMX dissolved in acetone is fixed at 2.17 wt% to maintain an initial saturation concentration in the solution. At a fixed pressure, the density of CO_2 decrease and the solubility of CO_2 in acetone also decrease as the temperature increase, thus resulting in a lowering of the degree of supersaturation in the solution. The volume-mean particle sizes of HMX were 12.9, 14.8, and 15.48 μm at 303, 313, and 323 K, respectively [24], [25].

The effect of the CO_2 addition rate on PSD of HMX is studied at 20 and 50 mL/min, at 303, 313, and 323 K. Fig. 13 shows the results indicating smaller particles are obtained at higher rate of CO_2 addition. The mean particle size decrease from 33.08 to 12.90 μm as the CO_2 addition rate is in-

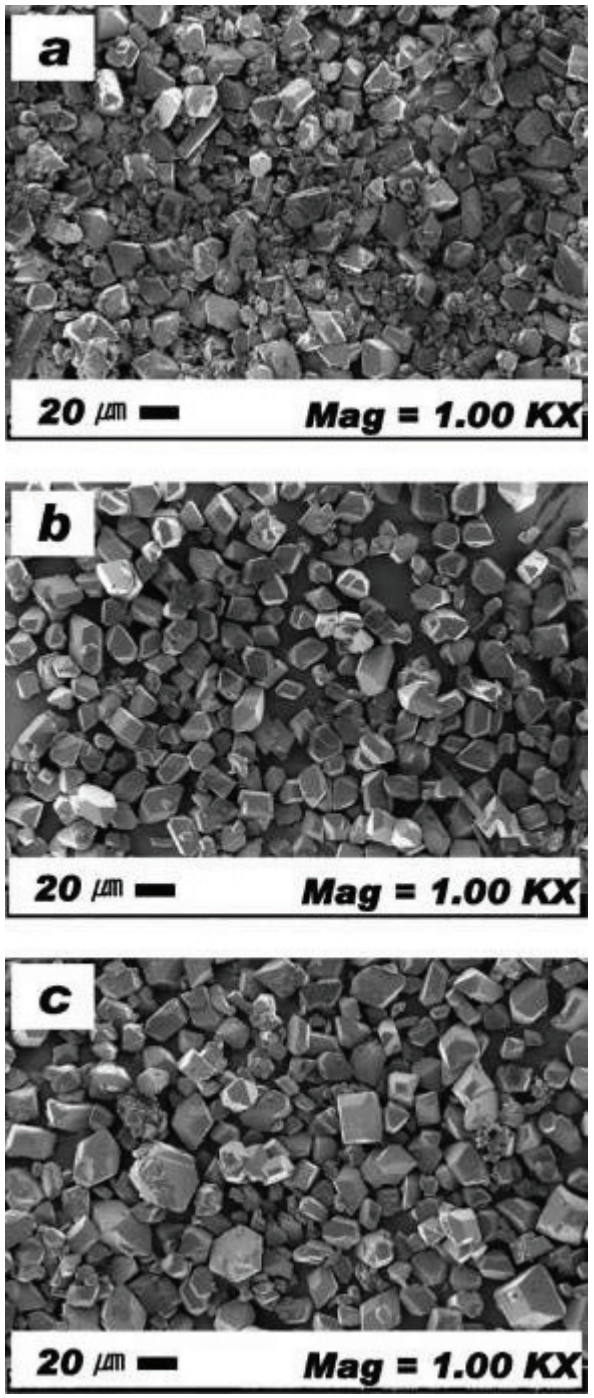

Figure 12: SEM images of HMX at (a) 303, (b) 313, and (c) 323 K

creased. The high addition rate of CO_2 induce high supersaturation level in a short time, leading to rapid nucleation. Therefore, the higher CO_2 addition rate produce smaller particles [24], [25].

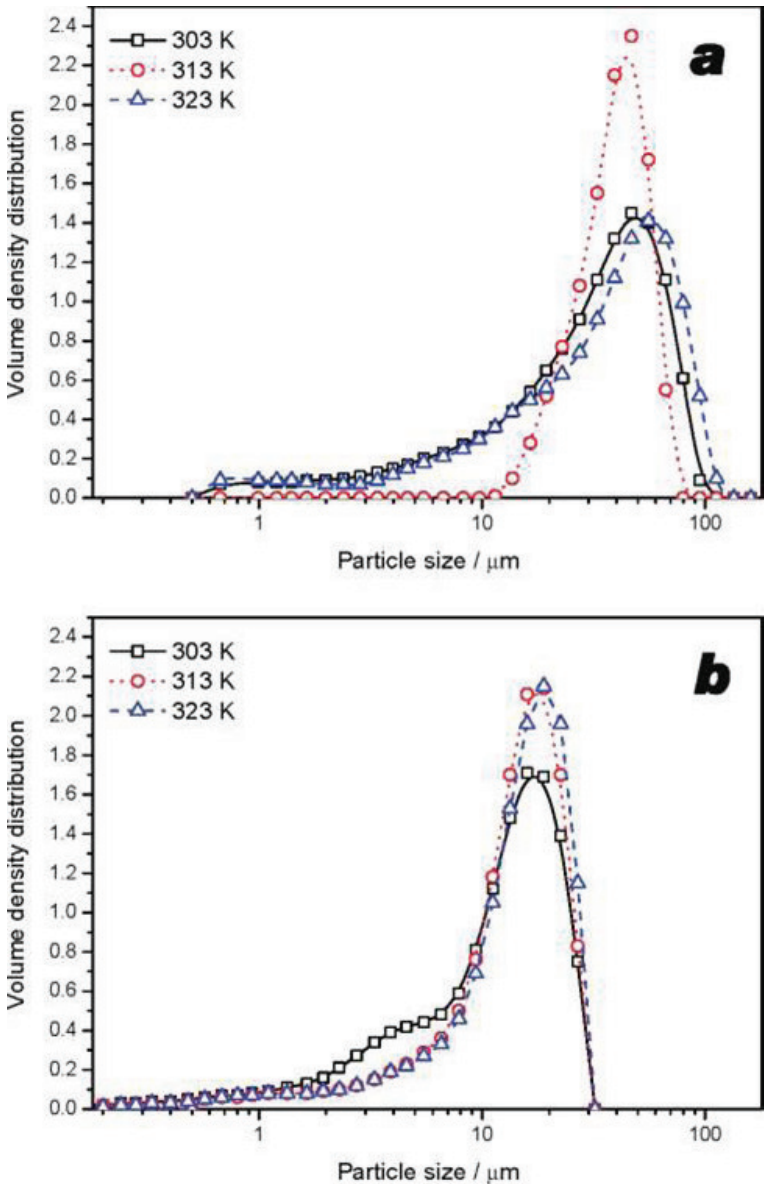

Figure 13: Effect of the CO_2 addition rate on PSD at (a) 20 and (b) 50 mL/min

Chapter 3

Modeling and Simulation for GAS process

In this chapter, a mathematical model for GAS process is presented using population balnce model (PBM). Population balnce model is first introduced to explain how particle distribution can be expressed in a mathematical form. PBM has a form of partial differential equation (PDE), requiring a particular numerical solution scheme. High resolution (HR) method is used because it is easy to implement and more accurate than other well-known methods. Finally, simulation results of particle size distribution are given in the last section.

3.1 Population balance model

The population balance model (PBM) is considered to be a statement of continuity. It tracks the change in particle size distribution as particles are born, die, grow, or leave a given control volume. In the population balance model, the one independent variable is the time, the other is the property coordinate, the particle size in most cases. Many chemical processes including polymerization, crystallization, and cell dynamics, are best described by population balance models [26].

$$\frac{\partial n(L,t)}{\partial t} + \frac{\partial \{G(L,t)n(L,t)\}}{\partial L} = q(L,t,f) \tag{3.1}$$

where $f(L,t)$ is the population density function which represents the particle size distribution given by $n(t,L)dL$, the number of particles in the size between L and $(L+dL)$ per unit volume of the solution, t denotes the time, L is an internal coordinate, $G(L,t)$ is the growth/dissolution rate, and $q(L,t,f)$ is the creation/depletion rate. The population density function changes with the time and internal coordinate so that it is in a form of partial differential equation.

The entities in the population can be molecules, cells, crystals, droplets, and so on. The internal coordinate L, often referred to as the size, is typically the characteristic length, volume, or mass, but it can also represent age, composition, and other characteristics of an entity in a distribution. The growth/dissolution rate $G(L,t)$ can be a function of size and other variables, such as the temperature and the concentration of chemical species in solution. The creation/depletion rate $q(L,t,f)$ includes nucleation, aggregation, agglomeration, breakage, attrition, and material leaving or entering the system. It can be a function of other variables including the distribution, which occurs in nucleation processes resulting from particle-particle interactions and in agglomeration processes. Many of these expressions involve integrals so that Eq. 3.1 is usually an integrodifferential equation [27].

$$\begin{aligned} \frac{\partial n(L,t)}{\partial t} + \frac{\partial\{G(L,t)n(L,t)\}}{\partial L} = \quad & \frac{1}{2}\int_0^\infty n(L-L',t)n(L',t)q(L-L',L')dL' \\ & -n(L,t)\int_0^\infty n(L',t)q(L,L')dL' + S(L) \end{aligned} \tag{3.2}$$

where $S(L)$ is rate at which particles of size L are nulceated and $q(L,L')$ is aggregation frequency. The growth/dissolution and creation/depletion rates, $G(L,t)$ and $q(L,t,f)$, are highly nonlinear functions of their arguments. The phases of nucleation, growth, and aggregation are illustrated in Fig. 14.

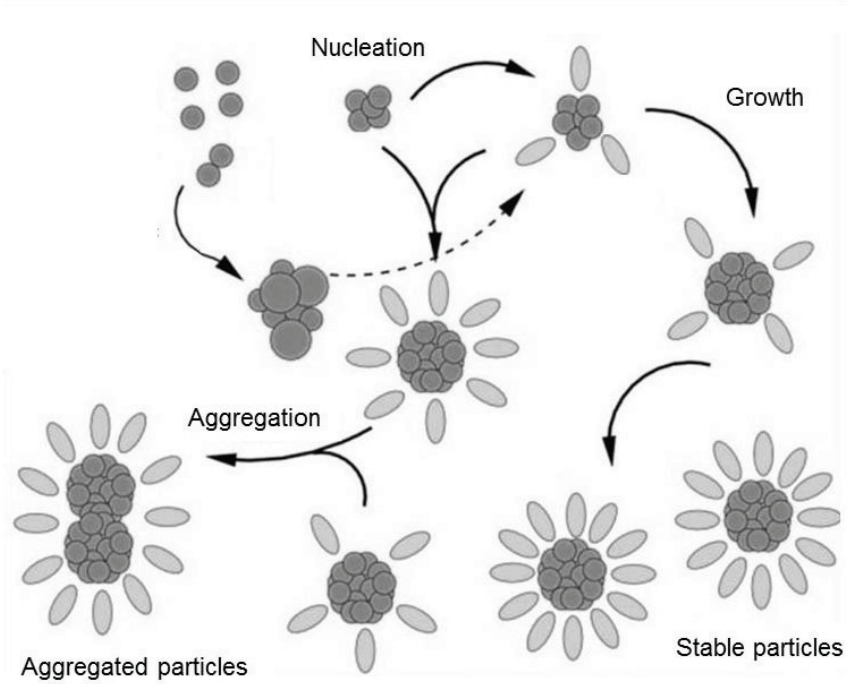

Figure 14: Nucleation, growth, and aggregation of particles

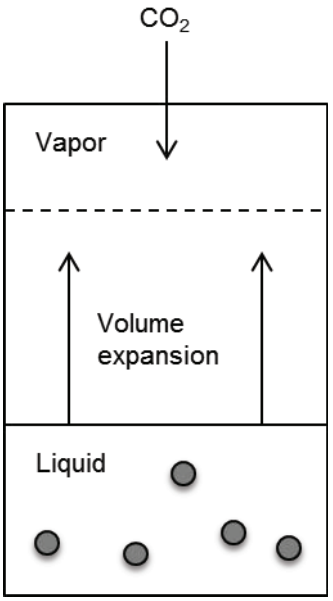

Figure 15: Schematic representation of GAS crystallization process

3.2 Mathematical model for GAS process

GAS process is schematically described in Fig. 15. A semibatch precipitator with constant volume, V, has one inlet to which the compressed CO_2 gas is injected. A solution with the dissolved solute to be crystallized is initially loaded in the precipitator. The solution volume expands as CO_2 gas is added. The dynamic model of GAS process is first developed by Dodds [28] using population balance model. The model accuracy is validated with the experimental results by Bakhbakhi [29] and Gunawan [30].

Several assumptions are made to derive a simplified model while retaining the basic dynamic behavior of the system. It is assumed that pressures at gas and liquid phases have the same value during crystallization and the temperature in the vessel is maintained at constant in spacetime so that no energy balance is needed. The growth rate, G, is size-independent. The mass transfer between gas and liquid phases is ignored and aggrega-

tion and breakage contribution of particles are also neglected. Disregard for aggregation and breakage of particles contributed to the birth and the death terms simplifies the population balance equation to

$$\frac{\partial n}{\partial t} + G\frac{\partial n}{\partial L} = 0 \tag{3.3}$$

The change of the particle size distribution with the liquid volume expansion is added to the left-hand side of the equation, thus the above equation can be rewritten as [11]

$$\frac{\partial n}{\partial t} + G\frac{\partial n}{\partial L} + \frac{n}{N_{\mathrm{L}} v_{\mathrm{L}}}\frac{d(N_{\mathrm{L}} v_{\mathrm{L}})}{dt} = 0 \tag{3.4}$$

where $N_L v_L$ indicates the liquid phase volume, given by the molar hold-ups in the liquid phase, N_L [mol], and the molar volume of the liquid phase, v_L [m^3/mol]. This term explains that the liquid phase volume rapidly changes and particle formation occurs in the liquid phase as CO_2 is injected to the crystallizer. Finally, populataion balance model describing GAS process can be obtained as a form of the partial differential equation.

The material balances on the antisolvent, the solvent, and the solute are given by the following equations

$$\frac{d(N_{\mathrm{L}} x_{\mathrm{A}} + N_{\mathrm{V}} y_{\mathrm{A}})}{dt} = Q_{\mathrm{A}} \tag{3.5}$$

$$\frac{d(N_{\mathrm{L}} x_{\mathrm{S}} + N_{\mathrm{V}} y_{\mathrm{S}})}{dt} = 0 \tag{3.6}$$

$$\frac{d(N_{\mathrm{L}} x_{\mathrm{P}} + N_{\mathrm{P}})}{dt} = 0 \tag{3.7}$$

where N_{V} [mol] and N_{P} [mol] are the molar hold-up in the gas and solid phases, respectively; x_i and y_i are mole fractions of component i in liquid and vapor phases, respectively (i = A, S, P); Q_{A} [mol/s] is the molar flow

rate of the antisolvent. N_P is given by

$$N_P = \frac{N_L v_L k_v m_3}{v_P} \tag{3.8}$$

where k_v, v_P, and m_3 are the volume shape factor, the molar volume of the solid phase, and the third moment of the population density function, respectively.

The third moment of the density function is calculated according to the general definition of the *i*th order moment of a distribution

$$m_i = \int_0^{L_{max}} L^i n(L) dL \quad (i = 3) \tag{3.9}$$

The initial conditions are given as follows

$$p = p_{atm} \tag{3.10}$$

$$n(0,L) = 0 \tag{3.11}$$

$$x_s N_L + y_S N_V = N_S^0 \tag{3.12}$$

$$x_P N_L = N_P^0 \tag{3.13}$$

where N_S^0 and N_P^0 are the initial molar amounts of solvent and solute, respectively.

The boundary condition for the partial differential equation is given as

$$n(t,0) = \frac{B}{G} \tag{3.14}$$

where B and G are the nucleation and growth rates, respectively, which are defined by constitutive equations for nucleation and growth kinetics of the system. General rate equations are considered here since crystallization

kinetics for GAS process has not been established yet. The nucleation rate is defined as the sum of two contributions, primary and secondary nucleations.

$$B = B' + B'' \quad (S > 1) \tag{3.15}$$

$$B' = 1.5D(c_{\mathrm{P}}N_{\mathrm{A}})^{7/3}\sqrt{\frac{\gamma}{kT}}\frac{v_{\mathrm{P}}}{N_{\mathrm{A}}} \times \exp\left[\frac{-16\pi}{3}\left(\frac{\gamma}{kT}\right)^3\left(\frac{v_{\mathrm{P}}}{N_{\mathrm{A}}}\right)\left(\frac{1}{\ln S}\right)^2\right] \tag{3.16}$$

$$B'' = \frac{\alpha'' a_{\mathrm{v}} D}{d_{\mathrm{M}}^4}\exp\left[-\pi\left(\frac{\gamma d_{\mathrm{M}}^2}{kT}\right)^2\frac{1}{\ln S}\right] \tag{3.17}$$

$$c_{\mathrm{P}} = \frac{x_{\mathrm{P}}}{v_{\mathrm{L}}} \tag{3.18}$$

$$a_{\mathrm{v}} = k_{\mathrm{a}} m_2 \tag{3.19}$$

$$D = \frac{kT}{2\pi\eta d_{\mathrm{M}}} \tag{3.20}$$

$$d_{\mathrm{M}} = \sqrt[3]{\frac{v_{\mathrm{P}}}{N_{\mathrm{A}}}} \tag{3.21}$$

$$G = K_{\mathrm{g}}(S-1)^g \quad (S > 1) \tag{3.22}$$

where B' is the primary nucleation rate, B'' is the secondary nucleation rate, respectively; c_{P} the solute concentration, k the Boltzman constant, γ the interfacial tension, N_{A} the Avogadro's number, α'' the secondary nucleation rate effectiveness factor, a_{v} the specific surface area, k_{a} the surface shape factor, m_2 the second moment of the density function, D the solute diffusion coefficient, η the dynamic viscosity, d_{M} the molecular diameter, and k_{g} the rate constant in the growth rate.

Thermodynamic behavior of GAS process is of importance because it determines the supersaturation of the solute which is the driving force for particle formation. The volumetric expansion of the liquid phase is de-

scribed by Peng-Robinson equation of state with quadratic mixing rules

$$P = \frac{RT}{v_\alpha - b_\alpha} - \frac{a_\alpha}{v_\alpha^2 + 2v_\alpha b_\alpha - b_\alpha^2} \quad (\alpha = \mathrm{L,V}) \tag{3.23}$$

$$a_\alpha = \sum_i \sum_j z_{i,\alpha} z_{j,\alpha} a_{ij} \quad (i,j = \mathrm{A,S}) \tag{3.24}$$

$$a_{ij} = (1 - k_{ij})\sqrt{a_i a_j} \tag{3.25}$$

$$b_\alpha = \sum_i \sum_j z_{i,\alpha} z_{j,\alpha} b_{ij} \tag{3.26}$$

$$b_{ij} = (1 - l_{ij}) \left(\frac{b_i + b_j}{2} \right) \tag{3.27}$$

where k_{ij} and l_{ij} are binary interaction coefficients and a_i and b_i are related to critical properties of the pure component

$$a_i = \frac{0.45724 R^2 T_\mathrm{c}^2}{P_\mathrm{c}} \left[1 + \alpha \left(1 - \left(\frac{T}{T_\mathrm{c}} \right)^{1/2} \right) \right]^2 \tag{3.28}$$

$$b_i = \frac{0.07780 R T_\mathrm{c}}{P_\mathrm{c}} \tag{3.29}$$

$$\alpha = 0.37464 + 1.54226\omega_i - 0.26992\omega_i^2 \tag{3.30}$$

where ω is the Pitzer acentric factor, T_c and P_c are the pure component's critical temperature and pressure, respectively. The fugacities in the liquid and vapor phases are expressed as

$$f_{i,\alpha} = z_{i,\alpha} \phi_{i,\alpha} P \tag{3.31}$$

and the fugacity coefficient, ϕ, is computed according to

$$\ln\phi_{j,\alpha} = \frac{b_k}{b_\alpha}\left(\frac{pv_\alpha}{RT}-1\right) - \ln\frac{p(v_\alpha-b_\alpha)}{RT} \pm \frac{a_\alpha}{2\sqrt{2}b_\alpha RT}\left[\frac{2\sum_i z_{i,\alpha}a_{i,j}}{a_\alpha} - \frac{b_j}{b_\alpha}\right] \times \ln\frac{v_\alpha+(1+\sqrt{2})b_\alpha}{v_\alpha+(1-\sqrt{2})b_\alpha} \tag{3.32}$$

The supersaturation is defined by the ratio of fugacities of the solid at the liquid and solid phases,

$$S = \frac{f_{\mathrm{P,L}}}{f_{\mathrm{P,P}}} \tag{3.33}$$

The fugacity of the solid at the solid phase, $f_{\mathrm{P,P}}$, is calculated by using Poynting correction factor

$$f_{\mathrm{P,P}} = f^0_{\mathrm{P,P}} \exp\left[\frac{v_{\mathrm{P}}(P-P_0)}{RT}\right] \tag{3.34}$$

$$f^0_{\mathrm{P,P}} = f_{\mathrm{P,L}}(P_0, T, x_0) \tag{3.35}$$

where P_0 and x_0 indicate a reference pressure and composition at the reference pressure, respectively.

3.3 High resolution method for solving PDE

A specific mathematical method is required to numerically solve the partial differential equation. The numerical simulation of the population balance model is especially challenging because the population density function, $n(L,t)$, extends over orders of magnitudes and the distribution is very sharp. We use a high resolution (HR) scheme because the HR algorithm can achieve improved accuracy with lower computational cost than other finite difference or finite volume methods for sharp distributions [30], [31].

The high resolution schemes were originally developed for compressible fluid dynamics and have been applied to aerodynamics, astrophysics, and related fields where shock waves occur [32]. They provide high or-

der accuracy while avoiding numerical diffusion and numerical dispersion which leads to nonphysical oscillations. Consider the nonlinear hyperbolic equation

$$\frac{\partial u(x,t)}{\partial t} + \frac{\partial}{\partial x} F(u) = 0 \tag{3.36}$$

where x and u denote the spatial and state variabels, respectively. This hyperbolic equation commonly rises in material, energy, and momentum balances. The numerical solution has some difficulties when the spatial derivative in Eq. 3.36 is large, that is, the function is very sharp. First-order methods may produce numerical diffusion and second-order methods cause numerical dispersion. High resolution method provide at least second-order accuracy where the solution is smooth and does not create numerical dispersion [30], [31].

HR algorithm is explained by using the one-dimensional homogeneous PBE which is written as

$$\frac{\partial f}{\partial t} + g\frac{\partial f}{\partial L} = 0 \tag{3.37}$$

where the growth rate, g $(g > 0)$, is size-independent. Let k and h denote the time and size intervals, respectively, and f_n^m denote an approximation of the average population density, expressed as

$$f_n^m \approx \frac{1}{\Delta x} \int_{(n-1)h}^{nh} f(x, mk)dx \tag{3.38}$$

where m, n are integers with respect to time and size such that $m \geq 0$ and $1 \leq n \leq N$. The high resolution algorithm with second-order accuracy has the form of [32]

$$\begin{aligned} f_n^{m+1} = \quad & f_n^m - \tfrac{kg}{h}(f_n^m - f_{n-1}^m) - \tfrac{kg}{2h}(1 - \tfrac{kg}{h}) \\ & \times \left[(f_{n+1}^m - f_n^m)\phi_n - (f_n^m - f_{n-1}^m)\phi_{n-1}\right] \end{aligned} \tag{3.39}$$

where the flux limiter function $\phi_n = \phi(\theta_n)$ depends on the degree of smooth-

ness of the distribution which is defined by

$$\theta_n = \frac{f_n^m - f_{n-1}^m}{f_{n+1}^m - f_n^m} \tag{3.40}$$

Many flux limiter functions have been proposed including the minmon, MC, and van Leer [32]. Each flux limiter leads to a different high resolution method. Van Leer flux limiter with full second-order accuracy is defined as [33]

$$\phi(\theta_n) = \frac{|\theta_n| + \theta_n}{1 + |\theta_n|} \tag{3.41}$$

Van Leer flux limiter is chosen since it does not show any numerical dispersion for one-dimensional problems [32].

Two HR methods are presentd by [34] for the homogeneous population balance equation with size-dependent growth which is

$$\frac{\partial f}{\partial t} + \frac{\partial (G(L)f)}{\partial L} = 0 \tag{3.42}$$

with the growth rate, $G(L)$. The first algorithm, HR1 is a formal second-order accurate method when no flux limiter is used. Here, the growth rates are evaluated at the endpoints of each grid cell.

$$\begin{aligned} f_n^{m+1} = \quad & f_n^m - \tfrac{k}{h}(G_n f_n^m - G_{n-1} f_{n-1}^m) \\ & - \tfrac{kG_n}{2h}\left(1 - \tfrac{kG_n}{h}\right)(f_{n+1}^m - f_n^m)\phi_n \\ & + \tfrac{kG_{n-1}}{2h}\left(1 - \tfrac{kG_{n-1}}{h}\right)(f_n^m - f_{n-1}^m)\phi_{n-1} \end{aligned} \tag{3.43}$$

where $G_n = G(nh)$. In the second algorithm, HR2, the growth rates are evaluated at the grid midpoitns [34]

$$\begin{aligned} f_n^{m+1} = \quad & f_n^m - \tfrac{k}{h}(G_{n-1/2} f_n^m - G_{n-3/2} f_{n-1}^m) \\ & - \tfrac{k}{2h}\left(1 - \tfrac{kG_n + 1/2}{h}\right)(G_{n+1/2} f_{n+1}^m - G_{n-1/2} f_n^m)\phi_n \\ & + \tfrac{k}{2h}\left(1 - \tfrac{kG_n - 1/2}{h}\right)(G_{n-1/2} f_{n+1}^m - G_{n-3/2} f_n^m)\phi_{n-1} \end{aligned} \tag{3.44}$$

The accuracy of solution can be different according to each HR algorithm. At the same time, calculation time also varies with the specific schemes. Therefore, a reasonable HR scheme has to be chosen considering the accuracy and the efficiency.

The above scheme with the first-order finite difference method (FDM) is compared for a simple population balance equation with the size-independent grow rate described by

$$\frac{\partial n(L,t)}{\partial t} + G\frac{\partial n(L,t)}{\partial L} = 0 \tag{3.45}$$

where G is 1.0 μm/s and the boundary condition is given as $n(0,t) = 0$. The initial distribution is [35]

$$n(L,0) = \begin{cases} 1 \times 10^{10} & \text{if } 10\,\mu\text{m} < L < 20\,\mu\text{m} \\ 0 & \text{else} \end{cases} \tag{3.46}$$

The crystal size range is $0 \leq L \leq 100$ μm which is discretized into 100 mesh elements. The analytical solution of this problem with initial profile $n(L,0) = n_0(L)$ is the initial profile which is translated by a distance Gt, that is,

$$n(L,t) = n_0(L - Gt) \tag{3.47}$$

The population densities for three solution approaches are compared in Fig. 16. The upper side and lower side figures are the distributions after 30 s and 60 s, respectively. The high resolution method shows better result than the finite defference method in both cases. It is also observed that the imprecision of FDM increases as the simulation time is longer while the accuracy of HR scheme does not change much.

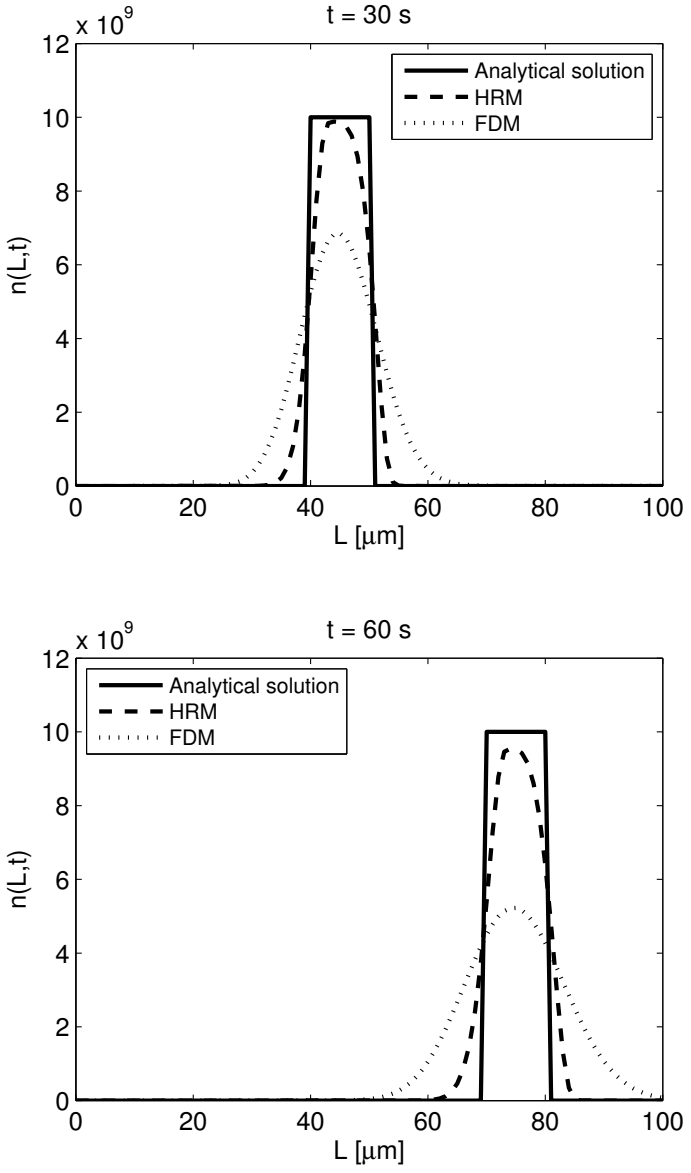

Figure 16: Comparison of solutions at 30 s and 60 s

3.4 Simulation results

The population balance mdoel of GAS process is solved using the second-order accurate fully one-sided upwind high resolution scheme and the limiting function ϕ uses the van Leer flux limiter [33] since it provides full second-order accuracy.

The dynamic model of GAS process is simulated for 100 seconds with constant CO_2 addition rates, 50, 100, 150, and 200 mL/min. The particle size ranges from 0 to 100 μm and the size of mesh is chosen to be 1 μm so that the total mesh number is 100. Calculations are performed by using the conmmercial software package MATLAB R2011b (7.13.0.564). The final particle size distributions at each CO_2 addition rate are shown in Fig. 17.

As shown in Fig. 17, the particle size distribution becomes narrower and the average particle size is reduced as the CO_2 addition rate increases. This is because fast CO_2 addition rate causes a sudden burst of nulceation while prevent the particle growth. Therefore, a great amount of small particles are formed, but they do not achieve the full growth. Mean sizes and variances of distributions are also provided in Table 3 and visuallized in Fig. 18. to quantitatively compare the results. Figs. 19-22 show 3D plots for

Table 3: Mean sizes and variances

CO_2 addition rate	Mean size	Variance
50 mL/min	86.7180	10.2243
100 mL/min	48.2915	6.7965
150 mL/min	35.4863	5.3524
200 mL/min	29.0861	4.5187

the four particle size distribuitons. They show how the distribution changes with both time and particle size, however, the final distribution is of only importance here because the system is a batch process which withdrawal of product is performed at once at the end of the batch.

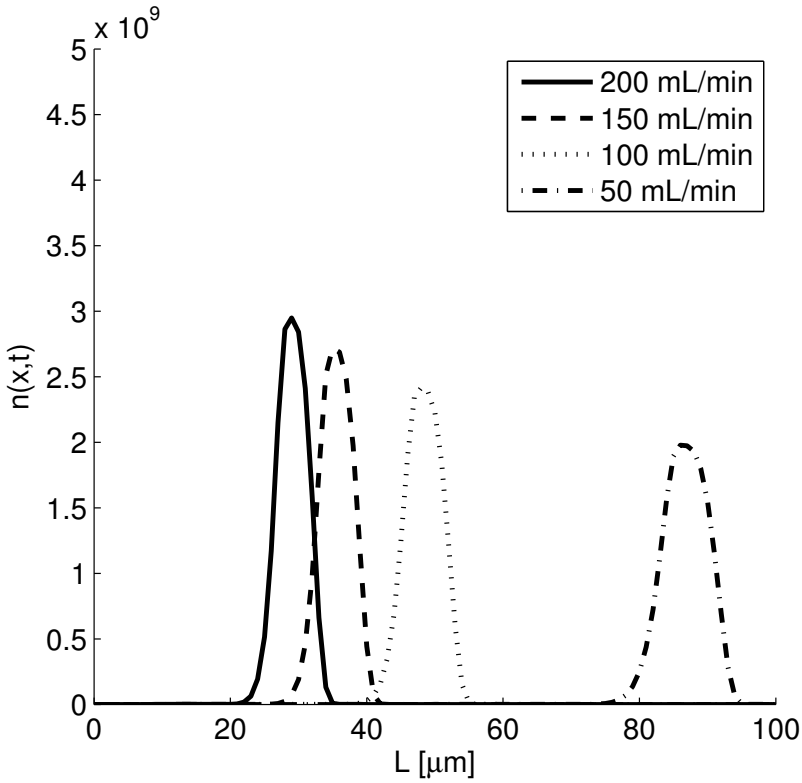

Figure 17: Particle size distributions

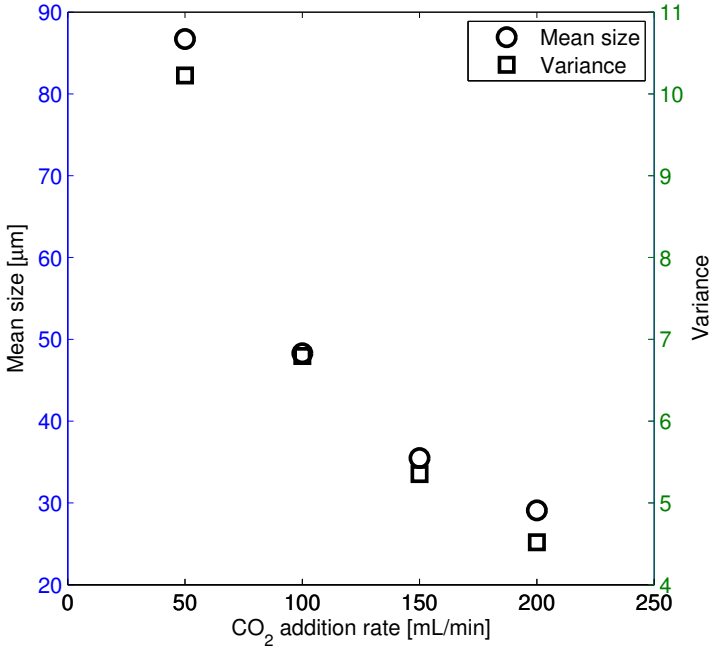

Figure 18: Mean sizes and variances

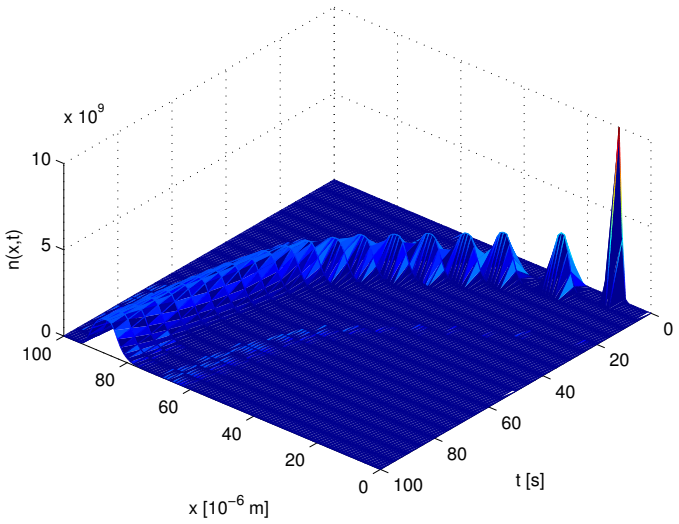

Figure 19: 3D plot of PSD at 50 mL/min

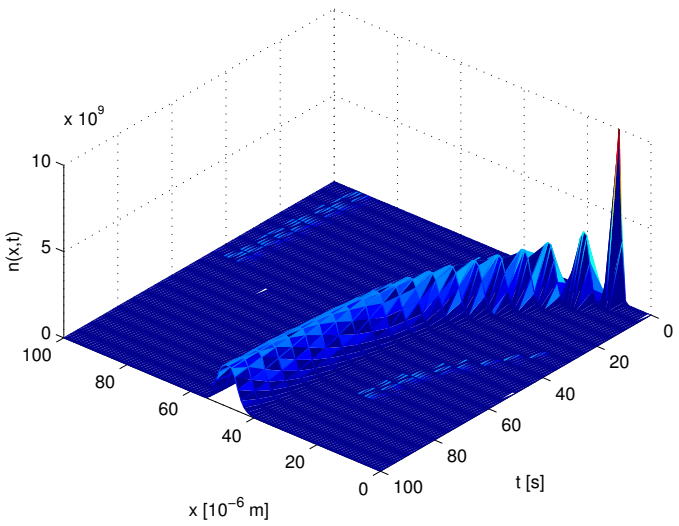

Figure 20: 3D plot of PSD at 100 mL/min

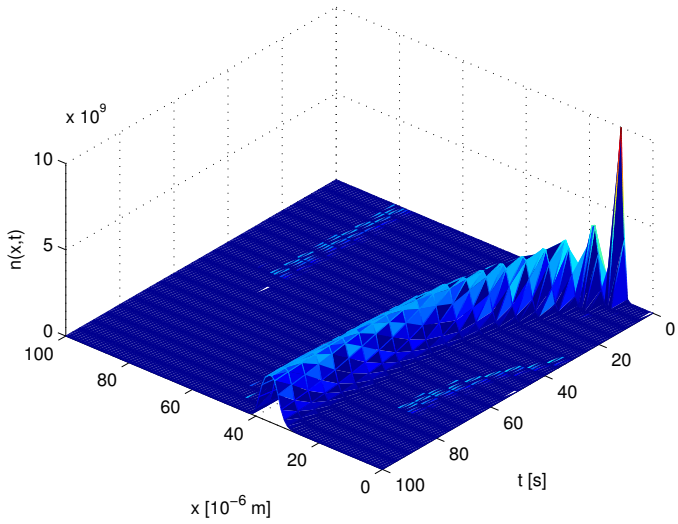

Figure 21: 3D plot of PSD at 150 mL/min

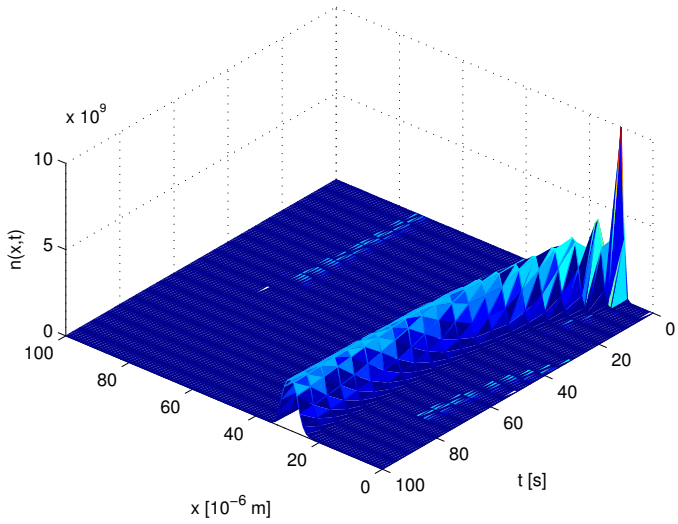

Figure 22: 3D plot of PSD at 200 mL/min

Chapter 4

Nonlinear Model Predictive Control for GAS Process

Obtaining fine crystals with a uniform distribution is a critical design problem in the GAS process system. It brings about the control issues. We here present two control approaches, model predictive control (MPC) to achieve the desired particle size and particle size distributio. At first, model predictive control (MPC) approaches are proposed in this chapter. MPC is applied because it is easy to handle constraints. Nonlinear MPC algorithm is used since GAS system shows highly nonlinear behavior.

In MPC algorithm, a dynamic process model of the plant is used to predict the effect of future action of the manipulated variables on the output. Therefore, the process model is the essential element of an MPC controller. Although models are not perfect, feedback can overcome some effects of poor models. The future moves of the manipulated variables are determined by optimization with the objective of minimizing the predicted error subject to operating constraints. The optimization is repeated at each sampling time based on updated measurements from the plant. Thus, the control problem is formulated as a dynamic optimization problem including the objectives and the constraints [36], [37].

The MPC concept was first appeared in chemical industries; Richalet et al. reported application of model predictive heuristic control to an industrial process in 1978 [38] and engineers from Shell described dynamic

matrix control (DMC) algorithm and reported optimization and constrained control of a catalytic cracking unit in 1979 [39], [40]. Since then, MPC has started to obtain its popularity in chemical process industries. They include a distillation column, a complex hydrocracker reactor, a fluid catalytic cracker, and other chemical petroleum refining operations as well as pulp and paper industries, a highly nonlinear batch reactor [41], [42], [43], [44], [45], [46]. This period is regarded the first decade of MPC, which is characterized by the increasing industrial growth, primarily in the oil and petrochemical industries.

In academic society, MPC has been applied to simple systems such as a mixing tank, heat exchanger, and a coupled distillation column under controlled conditions [47], [48], [49]. These applications are multivariable and constrained, which strongly motivated the development of a theoretical background of MPC. A second branch of MPC emerged and led to significant advances in understanding MPC algorithm including state-space interpretations/formulations and stability proofs. At the same time, the prosperity of the industrial MPC continued to succeed.

The third decade has started with the emergence of hybrid MPC. Essentially all processes contain discrete as well as continuous components: on/off valves, switches, logical overrides, and so forth. Some researchers have considered application of MPC in this environment [50], [51], [52], [53], [54] where MPC yielded a mixed integer linear programing (MILP) or a mixed integer quadratic programming (MIQP) problem to be solved on-line. It required much faster sampling rate than chemical process applications did since many hybrid systems are mechanical and mechatronic systems. Now MPC is opening up a new stage handling uncertainties in an optimal control problem by using approximate dynamic programming (ADP) [36], [37], [55].

We describe the fundamental linear and nonlinear MPC algorithms in the following two sections. Then, the results of nonlinear MPC of GAS

process are presented. The final product quality is improved by nonlinear MPC as shown in the results.

4.1 Model predictive control algorithm

Models

All the derivations in this paper will be carried out for general MIMO systems. Occasionally, in the interest of providing special insight SISO systems will be discussed separately. The idea of MPC is not limited to a particular system description, but the computation and implementation depend on the model representation. Depending on the context we will readily switch between state space, transfer matrix and convolution type models. The system to be described is assumed in state space by [40]

$$x(k) = Ax(k-1) + Bu(k-1) \tag{4.1}$$

$$y(k) = Cx(k) \tag{4.2}$$

For zero-initial conditions the equivalent transfer matrix representation is

$$y(z) = P(z)u(z) \tag{4.3}$$

where

$$P(z) \stackrel{\triangle}{=} C(zI)^{-1}B \tag{4.4}$$

Because most chemical engineering processes are open-loop stable our discussion will be limited to stable systems. The extension of the presented results to unstable systems is described elsewhere [56]. When A is stable, the inverse in Eq. 4.4 can be expanded into a Neuman series

$$P(z) = \sum_{i=0}^{\infty} CA^iBz^{-i-1} \tag{4.5}$$

$$P(z) \triangleq \sum_{i=1}^{\infty} H_i z^{-i} \tag{4.6}$$

where H_i are the impulse response coefficients, the magnitudes of which vanish as $i \to \infty$. Thus, in the time domain we have the truncated impulse response model

$$y(k) = \sum_{i=1}^{n} S_i u(k-i) = H_1 u(k-1) + H_2 u(k-2) + \cdots + H_n u(k-n) \tag{4.7}$$

and with the definitions

$$H_i = S_i - S_{i-1} \tag{4.8}$$

$$S_i = \sum_{j=1}^{i} H_j \tag{4.9}$$

the truncated step response model

$$y(k) = \sum_{i=1}^{n-1} S_i \Delta u(k-i) + S_n u(k-n) \tag{4.10}$$

where

$$\Delta u(k) = u(k) - u(k-1) \tag{4.11}$$

and S_i are the step response coefficients. Depending on the time delay structure of the system the leading step response coefficient matrices may be zero or have zero elements. Note that $\Delta u(k-i)$ instead of $u(k-i)$ appears in the model.

Dynamic matrix control (DMC)

The name "Model Predictive Control" arises from the manner in which the control law is computed as shown in Fig. 23. At the present time k the behavior of the process over a horizon p is considered. Using a model the process response to changes in the manipulated variable is predicted. The

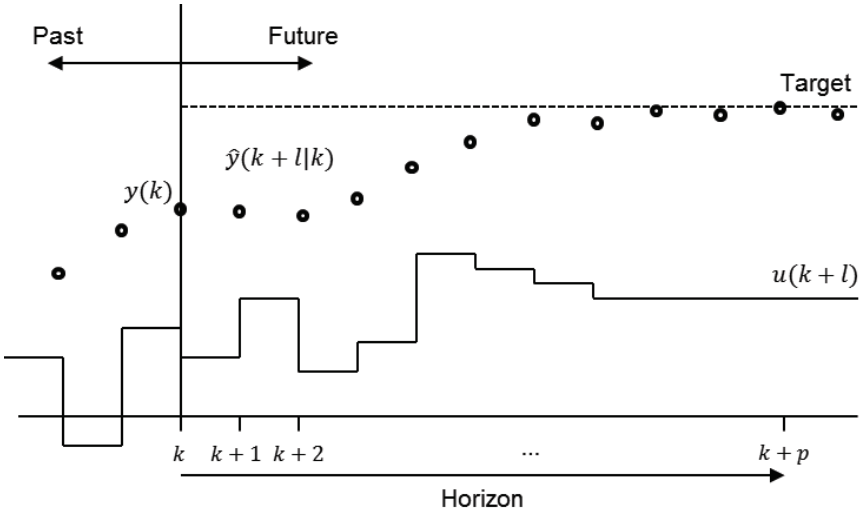

Figure 23: Moving horizon approach of MPC

moves of the manipulated variables are selected such that the predicted response has certain desirable characteristics. Only the first computed change in the manipulated variable is implemented. At time $k+1$ the computation is repeated with the horizon moved by one time interval. Dynamic matrix control (DMC) algorithm is derived as below.

There are three kinds of inputs, manipulated varialbe (u), measure disturbance (d), and unmearsured disturbance (ω_y). The system dynamics are represented as step response model. Define the state as the effect of past deviation and current bias of known inputs (u and d) on the future output behavior

$$\tilde{Y}(k) = \begin{bmatrix} y(k) \\ y(k+1) \\ \vdots \\ y(k+n-1) \end{bmatrix} \tag{4.12}$$

with

$$\Delta u(k) = \Delta u(k+1) = \cdots = 0$$
$$\Delta d(k) = \Delta d(k+1) = \cdots = 0$$
$$\omega_y(k) = \omega_y(k+1) = \cdots = 0$$

The predictin of output is expressed as

$$y(k+l|k) = \sum_{i=1}^{l} S_i \Delta u(k+l-i) + \sum_{i=l+1}^{n-1} S_i \Delta u(k+l-i) + S_n u(k+l-n) + \hat{d}(k+l|k) \tag{4.13}$$

$$d(k+l|k) = d(k|k) = y(k) - \sum_{i=1}^{n-1} S_i \Delta u(k-i) + S_n u(k+l-n) \tag{4.14}$$

where $y(k+l|k)$ is the predicted value of y at time $k+1$ based on information available at time k, $d(k+l|k)$ the predicted value of additive distrubances at process output at time $k+1$ based on information available at time k, $y(k)$ the measurement of y at time k, respectively. The prediction of output (Eq. 4.13) involves three terms on the right-hand side. The first term includes the present and all future moves of the manipulated variables which are to be determined so as to solve opimization. The second term includes only past values of the manipulated variables and is completely known at time k. The third term is the predicted disturbance $\hat{d}$ which is obtained from Eq. 4.7. At time k it is estimated as the difference between the measured output $y(k)$ and the output predicted from the model. In block diagram notation, Eq. 4.14 corresponds to a model $\tilde{\mathrm{P}}$ in parallel with the plant P (Fig. 24) with the resulting feedback signal equal to $d(k|k)$.

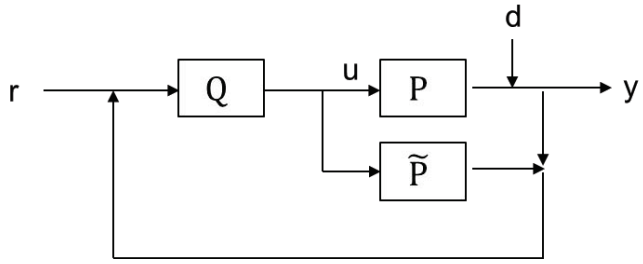

Figure 24: DMC structure

Multi-step prediction are then described by

$$\begin{bmatrix} y(k+1|k) \\ y(k+2|k) \\ y(k+3|k) \\ \vdots \\ y(k+p|k) \end{bmatrix} = \begin{bmatrix} \tilde{y}(k+1|k) \\ \tilde{y}(k+2|k) \\ \tilde{y}(k+3|k) \\ \vdots \\ \tilde{y}(k+p|k) \end{bmatrix} + \begin{bmatrix} S_1^d \\ S_2^d \\ S_3^d \\ \vdots \\ S_n^d \end{bmatrix} \Delta d(k) + \begin{bmatrix} y(k)-\tilde{y}(k|k) \\ y(k)-\tilde{y}(k|k) \\ y(k)-\tilde{y}(k|k) \\ \vdots \\ y(k)-\tilde{y}(k|k) \end{bmatrix}$$
$$+ \begin{bmatrix} S_1^u & 0 & \cdots & \cdots & 0 \\ S_2^u & S_1^u & 0 & \cdots & 0 \\ \vdots & \vdots & \ddots & \ddots & \vdots \\ S_m^u & S_{m-1}^u & \cdots & \cdots & S_1^u \\ \vdots & \vdots & \ddots & \ddots & \vdots \\ S_p^u & S_{p-1}^u & \cdots & \cdots & S_{p-m+1}^u \end{bmatrix} \begin{bmatrix} \Delta u(k|k) \\ \Delta u(k+1|k) \\ \Delta u(k+2|k) \\ \vdots \\ \Delta u(k+m-1|k) \end{bmatrix} \tag{4.15}$$

Several assumptions are made in the multi-step prediction: piece-wise constant disturbances, piece-wise constant signal (This makes it a feedback-based prediction), and only m input moves less than p ($m \leq p$). At time k, the manipulated variables are selected to minimize a quadratic objective

$$\begin{aligned} \min_{\Delta u} \quad & \textstyle\sum_{j=1}^{p} (r(k+i|k)-y(k+i|k))^T Q(r(k+i|k)-y(k+i|k)) \\ & + \textstyle\sum_{l=0}^{m-1} \Delta u^T(k+l|k) R \Delta u(k+l|k) \end{aligned} \tag{4.16}$$

subject to

$$\begin{aligned} & u_{\min} \leq u(k+l|k) \leq u_{\max} \\ & \Delta u(k+l|k) \leq \Delta u_{max}, \quad l = 0, \cdots, m-1 \\ & y_{\min} \leq y(k+j|k) \leq y_{\max}, \quad j = 1, \cdots, p \end{aligned} \tag{4.17}$$

where Q and R are weighting matirces, typically chosen as diagonal matrices; $u_{\min}$, $u_{\max}$, $y_{\min}$, and $y_{\max}$ are the minimun and maximum values of input and output variables, respectively. User-chosen parameters are the prediction horizon (p), control horizon (m), and weighting matrices in the objective function (Q and R). The above constrained objective function can be expressed as a quadratic program (QP)

$$\begin{aligned} & \min_{\Delta U} (\Delta U^T H \Delta U - g^T \Delta U) \\ & C\Delta U \geq c \end{aligned} \tag{4.18}$$

where

H : Hessian matrix
g : Gradient vector
C : Constraint matrix
c : Constraint vector
Δu : Decision variable

The QP is solved on-line at every time step. QPs are convex, therefore fundamentally tractable. This controller is represented by block Q in Fig. 24 [37].

4.2 MPC results of GAS process

A major limitation of linear MPC (LMPC) is that plant behavior is described by linear dynamic models. As a result, LMPC is inadequate for highly nonlinear processes and moderately nonlinear processes which have large operating regimes. This shortcoming coupled with increasingly stringent de-

mands on throughput and product quality has spurred the development of nonlinear model predictive control (NMPC).

NMPC is conceptually similar to its linear counterpart except that nonlinear dynamic models are used for process prediction and optimization.

Many processes are sufficiently nonlinear to preclude the successful application of LMPC technology. Such processes include highly nonlinear processes that operate near a fixed operating point (e.g. high-purity distillation columns) and moderately nonlinear process with large operating regimes (e.g. multi-grade polymer reactors). This has led to the development of nonlinear model predictive control (NMPC) in which a more accurate nonlinear model is used for process prediction and optimization. While NMPC offers the potential for improved process operation, it offers theoretical and practical problems which are considerably more challenging than those associated with LMPC. Many of these problems are associated with the nonlinear program which must be solved on-line at each sampling period to generate the control moves [57].

In this section, linear model predictive control and successive linearized model predictive control (sLMPC) are applied to GAS process and their results are compared.

Fig. 25 shows the result of LMPC. Prediction horizon and control horizon are chosen as 5 and 3, respectively. Simulation time and sampling time are 200 and 0.2, repectively. It is realized that the CO_2 addition rates are gradually increased satisfying constraints. The resulting PSD is much narrower when the system is controlled by MPC.

Successive linearized MPC is also applied to GAS process. The sLMPC improve control performance than LMPC as shown in Fig. 26. It is because GAS process is nonlinear system. The Mean sizes and variances are also given in Fig. 27.

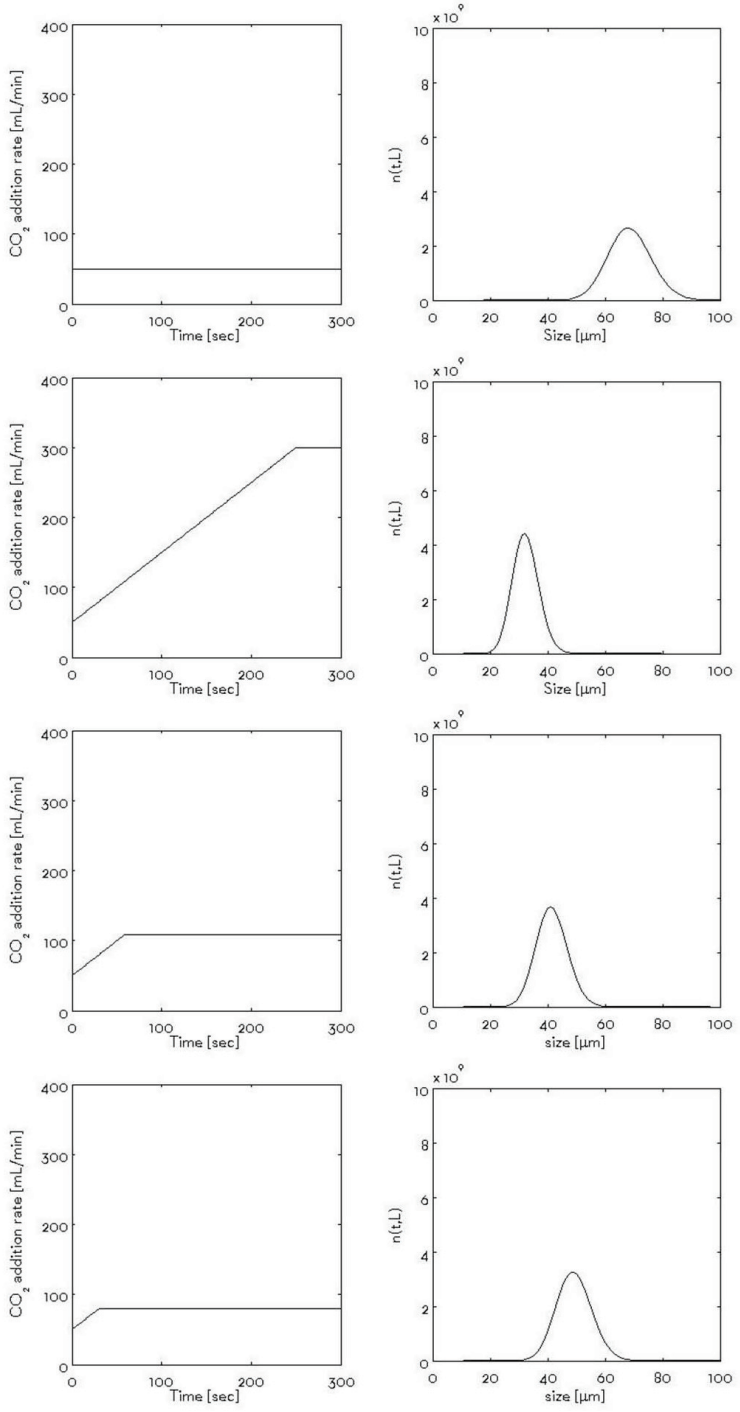

Figure 25: The results of LMPC

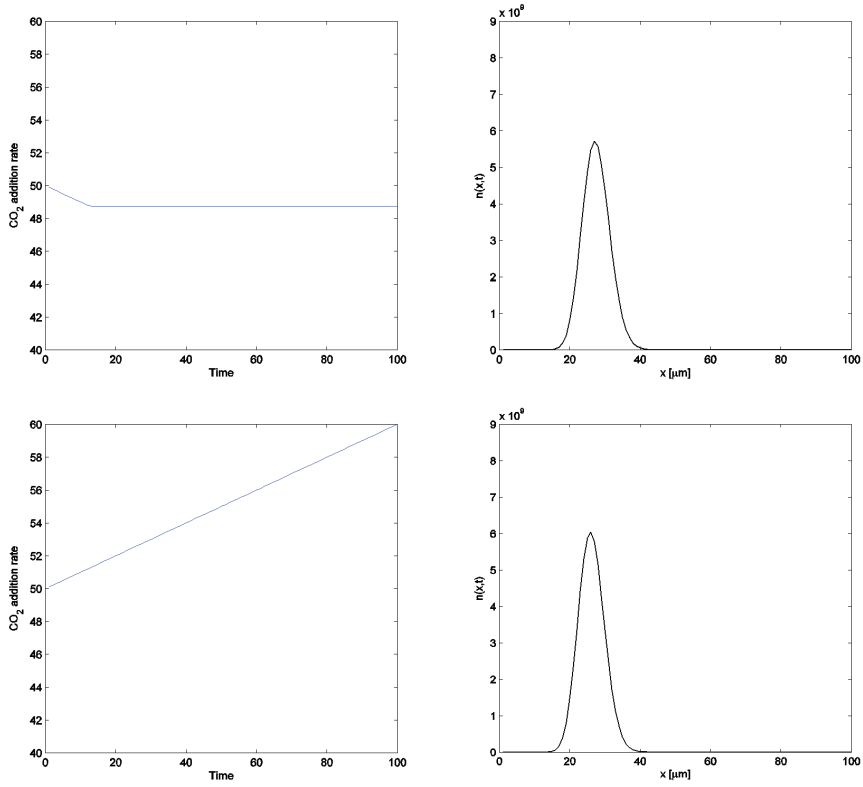

Figure 26: Comparison of LMPC and sLMPC

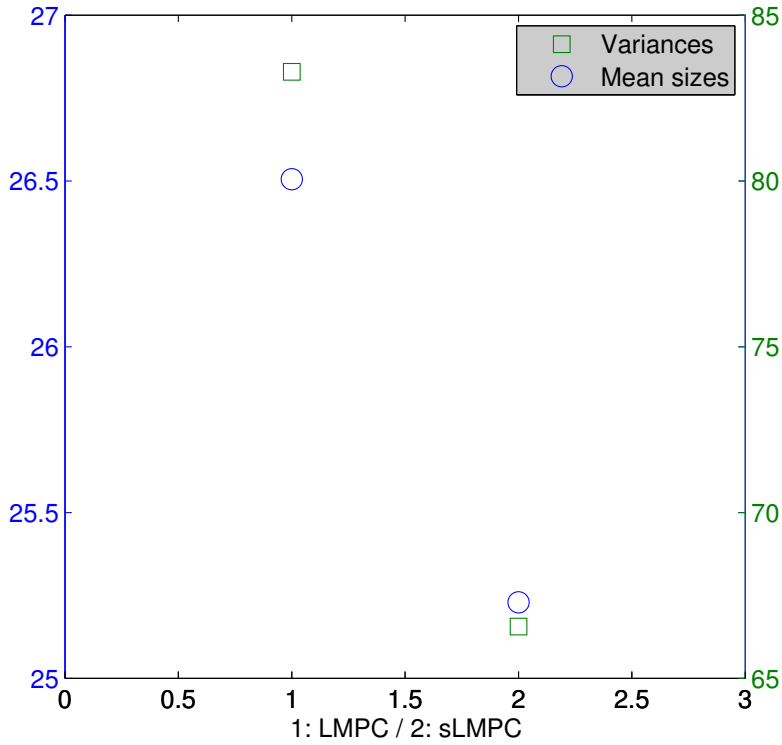

Figure 27: Mean sizes and Variances

Chapter 5

Concluding Remarks

In this thesis, gas antisolvent (GAS) recrystallization process is modeled to describe particle size distribution (PSD), simulated to investigate the effect of CO_2 addition rate on the final PSD, and controlled to obtain the desired PSD. GAS process has several advantages over conventional solution crystallization process. It does not produce toxic organic waste streams, is applicable to various solutes, and forms fine particles with uniform particle size distribution. HMX which is widely used as explosive is recrystallized using GAS process in the experiment. Experimental results show the particle size of HMX reduces as the CO_2 addition rate decreases.

Population balance model (PBM) is used to develop GAS process model describing the particle size distribution. PBM is a mathematical representation of PSD as particles are born, die, grow, or leave a given control volume. It involves two independent variables, one is the time and the other is the particle size, so that it has a form of partial differential equation (PDE). In GAS model, a term of liquid volume change with time is added since particles are formed in liquid phase. Several constitutive equations are also included; thermodynamic equations related to liquid volume expansion and nucleation and growth rates of particle kinetics.

GAS process model includes partial differential equation requiring a discretization method to numerically solve it. High resolution (HR) scheme is introduced because it provides high order accuracy while avoiding numerical diffusion and dispersion which lead to nonphysical oscillations. Van

Leer flux limiter is used as the limiting function to acquire full second-order accuracy. The method is tested using one-dimensional hyperbolic PDE and the results show better accuracy of HR scheme than finite difference model (FDM). Particle size is discretized to have 100 meshes and the process is simulated for 100 seconds. Simulation results show that the particle size is smaller and the PSD is more uniform as the CO_2 addition rate is faster.

Control issues of GAS process are quite challenging because the system is highly nonlinear and includes complex liquid-vapor equilibrium and particle kinetics. A model predictive control (MPC) approach is presented, which is well established control algorithm for controlling constrained multivariable processes. The process is controlled by two MPC schemes, linear MPC (LMPC) and successive linearized MPC (sLMPC), and the results are compared. They show control performance is improved when sLMPC is applied.

Bibliography

[1] D. A. Green, Du Pont Magazine Nov./Dec. (1988).

[2] P. Larsen, D. Patience, J. Rawlings, Industrial crystallization process control, Control Systems, IEEE 26 (4) (2006) 70–80.

[3] J. Jung, M. Perrut, Particle design using supercritical fluids: literature and patent survey, The Journal of Supercritical Fluids 20 (3) (2001) 179–219.

[4] Z. Knez, E. Weidner, Particles formation and particle design using supercritical fluids, Current Opinion in Solid State and Materials Science 7 (4) (2003) 353–361.

[5] D. Matson, J. Fulton, R. Petersen, R. Smith, Rapid expansion of supercritical fluid solutions: solute formation of powders, thin films, and fibers, Industrial & Engineering Chemistry Research 26 (11) (1987) 2298–2306.

[6] R. Petersen, D. Matson, R. Smith, The formation of polymer fibers from the rapid expansion of supercritical fluid solutions, Polymer Engineering & Science 27 (22) (2004) 1693–1697.

[7] E. Phillips, V. Stella, Rapid expansion from supercritical solutions: application to pharmaceutical processes, International Journal of Pharmaceutics 94 (1-3) (1993) 1–10.

[8] E. Berends, Supercritical crystallization: the RESS-process and the GAS-process, Technische Universiteit (1994).

[9] H. Ksibi, Effect of small capillaries on the hydrodynamic conditions in the ress process, Proc. 5th Supercri. Fluids 313.

[10] P. Gallagher, M. Coffey, V. Krukonis, N. Klasutis, Gas antisolvent recrystallization: new process to recrystallize compounds insoluble in supercritical fluids, ACS Symp. Ser, 406 (335) (1989) 3218. 3218.

[11] G. Muhrer, C. Lin, M. Mazzotti, Modeling the gas antisolvent recrystallization process, Industrial & Engineering Chemistry Research 41 (15) (2002) 3566–3579.

[12] I. Liau, M. McHugh, Supercritical fluid technology, Penninger, JML (1985) 415–434.

[13] R. Wissinger, M. Paulaitis, Swelling and sorption in polymer–co2 mixtures at elevated pressures, Journal of Polymer Science Part B: Polymer Physics 25 (12) (1987) 2497–2510.

[14] E. GULARI, W. Charles, Rheological properties of thermoplastics modified with supercritical gases, Proceedings of the 5th International Symposium on Supercrit2 ical Fluids. Atlanta, Georgia, USA (2000).

[15] Z. Nagy, R. Braatz, Advances and new directions in crystallization control, Annual Review of Chemical and Biomolecular Engineering 3 (2012) 55–75.

[16] J. Rawlings, S. Miller, W. Witkowski, Model identification and control of solution crystallization processes: A review, Industrial & Engineering Chemistry Research 32 (7) (1993) 1275–1296.

[17] J. Worlitschek, M. Mazzotti, Model-based optimization of particle size distribution in batch-cooling crystallization of paracetamol, Crystal Growth & Design 4 (5) (2004) 891–903.

[18] J. Corriou, S. Rohani, A new look at optimal control of a batch crystallizer, AIChE Journal 54 (12) (2008) 3188–3206.

[19] S. Chung, D. Ma, R. Braatz, Optimal seeding in batch crystallization, The Canadian Journal of Chemical Engineering 77 (3) (1999) 590–596.

[20] J. Ward, D. Mellichamp, M. Doherty, Choosing an operating policy for seeded batch crystallization, AIChE Journal 52 (6) (2006) 2046–2054.

[21] Z. Nagy, R. Braatz, Worst-case and distributional robustness analysis of finite-time control trajectories for nonlinear distributed parameter systems, Control Systems Technology, IEEE Transactions on 11 (5) (2003) 694–704.

[22] P. Larsen, J. Rawlings, N. Ferrier, An algorithm for analyzing noisy, in situ images of high-aspect-ratio crystals to monitor particle size distribution, Chemical Engineering Science 61 (16) (2006) 5236–5248.

[23] A. Mesbah, A. Kalbasenka, A. Huesman, H. Kramer, P. Van den Hof, Real-time dynamic optimization of batch crystallization processes, Proceedings of the 17th IFAC World Congress (2008) 3246–3251.

[24] B. Lee, S. Kim, B. Lee, H. Kim, H. Kim, Y.-W. Lee, Preparation of micronized β-hmx using supercritical carbon dioxide as antisolvent, Industrial & Engineering Chemistry Research 50 (15) (2011) 9107–9115.

[25] S. Kim, B. Lee, B. Lee, H. Kim, H. Kim, Y.-W. Lee, Recrystallization of cyclotetramethylenetetranitramine (HMX) using gas anti-solvent (GAS) process, The Journal of Supercritical Fluids 59 (2011) 108–116.

[26] D. Ramkrishna, Population balances: Theory and applications to particulate systems in engineering, Academic press (2000).

[27] S. Kumar, D. Ramkrishna, On the solution of population balance equations by discretization?i. a fixed pivot technique, Chemical Engineering Science 51 (8) (1996) 1311–1332.

[28] S. Dodds, J. Wood, P. Charpentier, Modeling of the gas-antisolvent (GAS) process for crystallization of beclomethasone dipropionate using carbon dioxide, Industrial & Engineering Chemistry Research 46 (24) (2007) 8009–8017.

[29] Y. Bakhbakhi, A discretized population balance for particle formation from gas antisolvent process: The combined lax-wendroff and crank-nicholson method, Computers & Chemical Engineering 33 (6) (2009) 1132–1140.

[30] R. Gunawan, I. Fusman, R. Braatz, High resolution algorithms for multidimensional population balance equations, AIChE Journal 50 (11) (2004) 2738–2749.

[31] S. Qamar, M. Elsner, I. Angelov, G. Warnecke, A. Seidel-Morgenstern, A comparative study of high resolution schemes for solving population balances in crystallization, Computers & Chemical Engineering 30 (6) (2006) 1119–1131.

[32] R. LeVeque, D. Mihalas, E. Dorfi, E. Müller, Computational Methods for Astrophysical Fluid Flow: Saas-Fee Advanced Course 27. Lecture Notes 1997 Swiss Society for Astrophysics and Astronomy, Springer 27 (1998).

[33] B. van Leer, Towards the ultimate conservative difference scheme, Journal of Computational Physics 135 (2) (1997) 229–248.

[34] R. LeVeque, Finite volume methods for hyperbolic problems, Vol. 31, Cambridge university press (2002).

[35] S. Motz, A. Mitrović, E. Gilles, Comparison of numerical methods for the simulation of dispersed phase systems, Chemical Engineering Science 57 (20) (2002) 4329–4344.

[36] J. Rawlings, Tutorial overview of model predictive control, Control Systems, IEEE 20 (3) (2000) 38–52.

[37] C. Garcia, D. Prett, M. Morari, Model predictive control: theory and practice - a survey, Automatica 25 (3) (1989) 335–348.

[38] J. Richalet, A. Rault, J. Testud, J. Papon, Model predictive heuristic control: Applications to industrial processes, Automatica 14 (5) (1978) 413–428.

[39] C. Cutler, B. Ramaker, Dynamic matrix control-a computer control algorithm, Proceedings of the Joint Automatic Control Conference 1 (1980).

[40] D. Prett, R. Gillette, Optimization and constrained multivariable control of a catalytic cracking unit, Proceedings of the Joint Automatic Control Conference 1 (1980).

[41] R. Mehra, R. Rouhani, J. Eterno, J. Richalet, A. Rault, Model algorithmic control: review and recent developments, Proceedings of the Engineering Foundation Conference on Chemical Process Control II, Sea Island, GA (1982) 287–310.

[42] C. Garcia, Quadratic dynamic matrix control of nonlinear processes: An application to a batch reaction process, AIChE annual meeting, San F rancisco (1984).

[43] T. Matsko, Internal model control for chemical recovery, Chemical Engineering Progress 81 (12) (1985) 46–51.

[44] C. Cutler, R. Hawkins, Constrained multivariable control of a hydrocracker reactor, American Control Conference, 1987, IEEE (1987) 1014–1020.

[45] G. Martin, J. Caldwell, T. Ayral, Predictive control applications for the petroleum refining industry, Petroleum Refining Conference, Tokyo, Japan, 1986.

[46] J. Caldwell, G. Martin, On-line analyzer predictive control, Sixth Annual Control Expo Conf, Rosemont, IL, (1987) 19–21.

[47] Y. Arkun, W. Canney, J. Hollett, M. Morari, Experimental study of internal model control, Industrial & Engineering Chemistry Process Design and Development 25 (1) (1986) 102–108.

[48] K. Levien, Studies in the design and control of coupled distillation columns, Vol. 1, University of Wisconsin–Madison, (1985).

[49] J. Parrish, C. Brosilow, Inferential control applications, Automatica 21 (5) (1985) 527–538.

[50] O. Slupphaug, B. Foss, Model predictive control for a class of hybrid systems, Proceedings European Control Conference, Citeseer, (1997).

[51] O. Slupphaug, On robust constrained nonlinear control and hybrid control: Bmi and mpc based state-feedback schemes, Ph.D dissertation, Norwegian University of Science and Technology.

[52] A. Bemporad, M. Morari, Predictive control of constrained hybrid systems, Nonlinear model predictive control (2000) 71–98.

[53] A. Bemporad, M. Morari, et al., Control of systems integrating logic, dynamics, and constraints, Automatica 35 (3) (1999) 407–427.

[54] D. Mignone, A. Bemporad, M. Morari, A framework for control, fault detection, state estimation, and verification of hybrid systems, American Control Conference, 1999, IEEE 1 (1999), 134–138.

[55] J. Lee, Model predictive control: Review of the three decades of development, International Journal of Control, Automation and Systems 9 (3) (2011) 415–424.

[56] M. Morari, E. Zafiriou, Robust process control, Morari (1989).

[57] M. Henson, Nonlinear model predictive control: current status and future directions, Computers & Chemical Engineering 23 (2) (1998) 187–202.

초 록

결정화 공정은 폴리머, 제약, 염료 제조 등의 화학산업에서 중요한 역할을 해오고 있으며 석유화학산업의 분리, 정제 단계에서 필수적으로 사용되는 공정 단위이다. 그러나 기존의 결정화 공정은 유독한 폐용매의 생성과 이 용매에 의한 결정의 순도 감소라는 문제점을 가지고 있다. 따라서 이러한 단점을 극복한 초임계 유체를 이용한 결정화 공정이 주목을 받고 있다. 이 공정들은 주용매로 이산화탄소 기체를 이용하기 때문에 환경적으로 큰 문제가 없고 다양한 종류의 물질에 적용이 가능하며 비교적 온화한 조건에서 운전이 가능하다. Rapid expansion of supercritical solution (RESS), gas anti-solvent (GAS) process, particles from gas-saturated solutions (PGSS) 등이 이에 포함된다.

이 중 특히 GAS 공정은 역용매인 이산화탄소의 주입과 함께 용액에서의 고체의 용해도가 급격히 감소함에 따라 매우 빠르게 높은 수준의 과포화도를 얻을 수 있다. 이것은 이산화탄소의 용해와 용매의 증발 과정에서 이산화탄소의 물질 전달과 용매의 물질전달이 동시에 일어나기 때문이다. 따라서 균일한 결정 핵이 생성되고 거의 동시에 결정화가 진행되어 균일한 입자크기분포와 형상을 가진 매우 미세한 입자들을 얻을 수 있다.

본 연구에서는 GAS 공정의 동적 모델링과 균일한 입자크기분포를 얻기 위한 제어 기법들에 대해 살펴본다. 우선 GAS 공정의 입자크기분포를 나타내기 위해 군집균형모델 (population balance model, PBM)을 이용한 수학적 모델을 제시하였다. 이 모델은 편미분 방정식과 상미분 방정식, 이와 관련된 대수식들로 이루어져 있기 때문에 편미분 방정식을 풀기 위한 이산화 기법이 필요하다. 여기서는 high resolution (HR) 기법을 제시하였다. 이 방법은 잘 알려진 다른 이산화 기법들에 비해 적용이 간단하고 좀더 개선된 정확도를 보인다. HR 기법으로 시뮬레이션을 수행하고 입자크기분포에 대한 이산화탄소 주입 속도의 영향을 살펴보았다. 시뮬레이션 결과, 이산화탄소 주입속

도가 50 , 100, 150, 200 mL/min으로 증가함에 따라 입자의 평균크기는 86.7180, 48.2915, 35.4863, 29.0861 μm로 감소하고, 입자크기분포의 분산은 10.2243, 6.7965, 5.3524, 4.5187로 감소한다.

GAS 공정은 매우 비선형적이고 핵 생성과 결정 성장과 같은 복잡한 결정화 kinetics을 포함하고 있기 때문에 이 공정의 제어 문제는 매우 까다롭다. 액체역용매결정화공정의 제어는 어느 정도 연구가 진행되었지만 기체 역용매 결정화 공정의 제어는 아직까지 많이 연구되지 않았다. 기체역용매결정화공정의 경우 액체-기체 상평형까지 고려해야 하기 때문에 좀더 어려운 문제가 된다. 여기서는 모델예측제어 (model predictive control, MPC) 기법을 이용하여 GAS 공정을 제어하였다.

주요어 : 기체 역용매 재결정화 공정, 군집균형모델, 모델예측제어
학번 : 2011-21062